

# Kinetics and Mechanisms of Oxygen Transfer in the Reaction of *p*-Cyano-*N,N*-dimethylaniline *N*-Oxide with Metalloporphyrin Salts. 2.<sup>1</sup> Amine Oxidation and Oxygen Transfer to Hydrocarbon Substrates Accompanying the Reaction of *p*-Cyano-*N,N*-dimethylaniline *N*-Oxide with *meso*-(Tetraphenylporphinato)iron(III) Chloride

C. Michael Dicken, Fu-Lung Lu, Michael W. Nee, and Thomas C. Bruice\*

Contribution from the Department of Chemistry, University of California at Santa Barbara, Santa Barbara, California 93106. Received February 12, 1985

**Abstract:** The catalysis of the decomposition of *p*-cyano-*N,N*-dimethylaniline *N*-oxide (NO) with *meso*-(tetraphenylporphinato)iron(III) chloride [(TPP)Fe<sup>III</sup>Cl] has been studied at 25 °C in CH<sub>2</sub>Cl<sub>2</sub> with [NO]<sub>0</sub> = 5.0 × 10<sup>-4</sup> to 8.0 × 10<sup>-3</sup> M > [(TPP)Fe<sup>III</sup>Cl]<sub>0</sub> = 3.0 × 10<sup>-5</sup> to 5.0 × 10<sup>-4</sup> M. The iron(III) porphyrin catalyst was shown to be unaltered in catalytic efficiency to 120 turnovers (the highest examined). The influence of O<sub>2</sub> and the purity of solvent upon the kinetics of the reactions and products obtained have been assessed. In the absence of an oxidizable substrate, NO gives way to the following products: *p*-cyano-*N,N*-dimethylaniline (DA), 52% yield; *p*-cyano-*N*-methylaniline (MA), 25% yield; *N*-formyl-*p*-cyano-*N*-methylaniline (FA), 4% yield; *p*-cyanoaniline (A), 2% yield; *N,N'*-dimethyl-*N,N'*-bis(*p*-cyanophenyl)hydrazine (H), 12% yield; *N,N'*-bis(*p*-cyanophenyl)-*N*-methylmethylenediamine (MD), 6% yield; and CH<sub>2</sub>O, 11% yield. The major portion of the products (i.e., DA, MA, H and MD) absorb appreciably at 320 nm where absorbance by (TPP)Fe<sup>III</sup>Cl is minimal. The formation of products was followed spectrophotometrically at 320 nm and by HPLC at 280 and 320 nm. Both means were found to be in quantitative agreement. Spectral monitoring of the increase in A<sub>320</sub> showed that the first-order decomposition of the *N*-oxide was independent of [NO]<sub>0</sub> but increases with an increase in [(TPP)Fe<sup>III</sup>Cl]<sub>0</sub>. The appearance of DA, MA, FA, MD, and CH<sub>2</sub>O also followed the first-order rate law, while the formation of the products H and A are characterized by a lag period followed by a constantly accelerated formation ending abruptly with the consumption of the *N*-oxide. Of the various products, only A exhibited inhibition of the kinetics for decomposition of *N*-oxide by (TPP)Fe<sup>III</sup>Cl. At the concentration formed in the kinetic experiment, however, A is not inhibiting. The rate constant for "oxygen" transfer from NO to (TPP)Fe<sup>III</sup>Cl to form [(TPP)(Cl)Fe<sup>IV</sup>=O]<sup>+</sup> was determined by trapping this species with 2,4,6-tri-*tert*-butylphenol (TBPH). In the presence of TBPH trap, DA is formed in 100% yield, showing that the other decomposition products of the *N*-oxide arise via stepwise oxidation of DA by [(TPP)(Cl)Fe<sup>IV</sup>=O]<sup>+</sup>. An intermolecular deuterium kinetic isotope effect of unity was obtained by comparison of the initial rate constants for the reactions of *p*-NCC<sub>6</sub>H<sub>4</sub>N<sup>+</sup>(CH<sub>3</sub>)<sub>2</sub>O<sup>-</sup>/*p*-NCC<sub>6</sub>H<sub>4</sub>N<sup>+</sup>(CD<sub>3</sub>)<sub>2</sub>O<sup>-</sup>. A discriminatory intramolecular deuterium isotope effect of 4.5 was observed when *p*-NCC<sub>6</sub>H<sub>4</sub>N<sup>+</sup>(CH<sub>3</sub>)(CD<sub>3</sub>)O<sup>-</sup> was used and the formation of *p*-NCC<sub>6</sub>H<sub>4</sub>NH(CD<sub>3</sub>)/*p*-NCC<sub>6</sub>H<sub>4</sub>NH(CH<sub>3</sub>) was monitored. The isotope effects are in agreement with the finding that rate-determining oxygen transfer from NO to (TPP)Fe<sup>III</sup>Cl is followed by demethylation of DA. A variety of alkenes and cyclohexane are shown to compete with DA as substrates. With these, the yields of epoxidation and/or hydroxylation products are comparable to those reported previously when iodosylbenzene was used as the oxygen source under similar conditions. The stereospecificity seen with iodosylbenzene is also evidenced with NO. At 1.0 M 2,3-dimethyl-2-butene, DA and tetramethylethylene oxide are both formed in 100% yield based upon [NO]<sub>0</sub> while the rate of the reaction is the same as in the absence of alkene. Therefore, at this concentration, this alkene serves as a trap for [(TPP)(Cl)Fe<sup>IV</sup>=O]<sup>+</sup>. Since a molecule of substrate (DA) is always generated with each molecule of [(TPP)(Cl)Fe<sup>IV</sup>=O]<sup>+</sup> formed, the [(TPP)(Cl)Fe<sup>IV</sup>=O]<sup>+</sup> species does not exist long enough to bring about the decomposition of the iron porphyrin catalyst. Yet, external substrates, such as alkene, compete with DA for the oxidant. The protective action of cogenerative DA is amplified by the fact that its oxidation to the products FA, MA, A, H, and MD requires a number of [(TPP)(Cl)Fe<sup>IV</sup>=O]<sup>+</sup> species. Similarities and differences in the reaction of (TPP)Fe<sup>III</sup>Cl and (TPP)Mn<sup>III</sup>Cl with NO are discussed. The experimental data concerning the stepwise oxidation of DA to yield the various oxidation products are discussed in terms of the most probable mechanisms. Computer simulation of the reaction of NO with (TPP)Fe<sup>III</sup>Cl to yield DA, FA, MA, H, A, and MD as products has been based upon the reactions and rate constants of Scheme I. This simulation successfully provides the correct percent yields of the multiple products, their individual rates of formation, and the kinetic observations which accompany changes in initial concentrations of reactants and additions of reaction products to the reaction solution before initiation of reactions. Also, the simulation allows rationalization of the rapid changes in the Soret band of (TPP)Fe<sup>III</sup>Cl (A<sub>410</sub>) which occur on initiation of the reaction of (TPP)Fe<sup>III</sup>Cl with NO. The second-order rate constants for epoxidation of a number of hydrocarbons by [(TPP)(Cl)Fe<sup>IV</sup>=O]<sup>+</sup> have been calculated and compared to the rate constants for epoxidation by MCPBA. Epoxidation by [(TPP)(Cl)Fe<sup>IV</sup>=O]<sup>+</sup> is more rapid and less sensitive to the nucleophilicity of the alkene than is epoxidation by the percarboxylic acid.

Iodosylbenzene, organic peroxyacids, and hydroperoxides have been employed with *meso*-(tetraphenylporphinato)iron(III) chloride [(TPP)Fe<sup>III</sup>Cl] to model the oxidation reactions of the cytochrome P-450 enzymes.<sup>2</sup> The higher valent states of the iron porphyrin to be considered in these reactions consists of porphyrin π-cation-radical complexes of "oxygen"-ligated iron(III) and iron(IV) species (most likely structures being [(TPP)(Cl)-Fe<sup>III</sup>OH]<sup>+</sup> and [(TPP)(Cl)Fe<sup>IV</sup>=O]<sup>+</sup>).<sup>2g,2h,3</sup> The reaction of (TPP)Fe<sup>III</sup>Cl with iodosylbenzene may be written as in eq 1. The

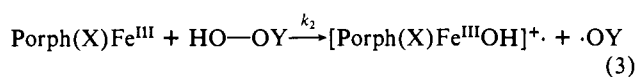
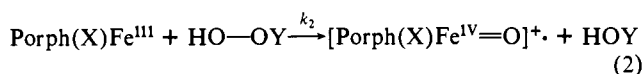


reaction of peroxy-carboxylic acids and organic hydroperoxides with (porphinato)iron(III) salts may occur by either heterolytic

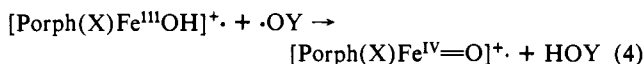
(1) Part I. Powell, M. F.; Pai, E. F.; Bruice, T. C. *J. Am. Chem. Soc.* **1984**, *106*, 3277.

(2) (a) Groves, J. T.; Nemo, T. E.; Myers, R. S. *J. Am. Chem. Soc.* **1979**, *101*, 1032. (b) Chang, C. K.; Kuo, M.-S. *Ibid.* **1979**, *101*, 3413. (c) Mansuy, D.; Bartoli, J.-F.; Chottard, J.-C.; Lange, M. *Angew. Chem., Int. Ed. Engl.* **1980**, *19*, 909. (d) Mansuy, D.; Dansette, P. M.; Pecquet, F.; Chottard, J.-C. *Biochem. Biophys. Res. Commun.* **1980**, *96*, 433. (e) Gold, A.; Ivey, W.; Brown, M. *J. Chem. Soc., Chem. Commun.* **1981**, 293. (f) Chang, C. K.; Ebina, F. *Ibid.* **1981**, 778. (g) Groves, J. T.; Haushalter, R. C.; Nakamura, M.; Nemo, T. E.; Evans, B. J. *J. Am. Chem. Soc.* **1981**, *103*, 2884. (h) Groves, J. T.; Quinn, R.; McMurry, T. J.; Lang, G.; Boso, B. *J. Chem. Soc., Chem. Commun.* **1984**, 1455.

(eq 2) or homolytic (eq 3) cleavage of the O—O bond and the

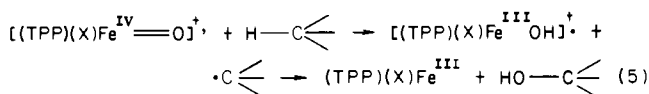


higher valent porphinato iron species so generated may be trapped by 2,4,6-*tert*-butylphenol.<sup>4</sup> For the homolytic reaction, the  $\cdot\text{OY}$  species may react with a substrate or undergo further reduction (eq 4). Using (TPP)Fe<sup>III</sup>Cl and a series of peroxy-



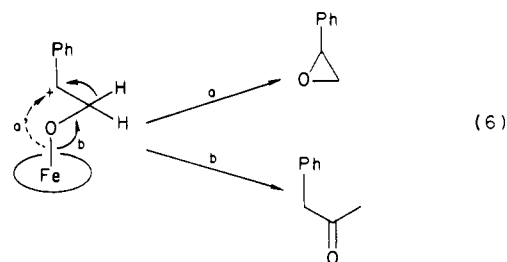
carboxylic acids and hydroperoxides in CH<sub>3</sub>OH, a plot of the log of the second-order rate constant for "oxygen" transfer ( $k_2$  of eq 2 and 3) vs.  $\text{p}K_a$  of YOH was found to be linear with the slope ( $\beta_{\text{LG}}$ ) of -0.35 up to a  $\text{p}K_a$  of YOH of ~11 where a break in the linear free energy relationship occurs. Thus, those hydroperoxides derived from aliphatic alcohols show little dependence of  $\log k_2$  upon the  $\text{p}K_a$  of YOH.<sup>5</sup> Since organic peroxy-carboxylic acids undergo heterolytic O—O bond cleavage<sup>4</sup> on reaction with (TPP)Fe<sup>III</sup>Cl, it follows that hydroperoxides derived from alcohols of  $\text{p}K_a$  less than ~11 also undergo heterolytic O—O bond cleavage (eq 4), while those hydroperoxides derived from less acidic alcohols (hydroperoxides devoid of strongly electron-withdrawing substituents on the  $\alpha$  carbon, such as all common hydroperoxides) must transfer oxygen by another mechanism, i.e., homolysis, eq 4. It is yet to be determined if and how the nature of the porphyrin, solvent, etc., determines the competition between heterolytic and homolytic oxygen transfer. It is known that the replacement of iron(III) by other metal ions results in a profound change in the mechanism. Thus, (TPP)Cr<sup>III</sup>Cl in CH<sub>2</sub>Cl<sub>2</sub> reacts with all peroxy-carboxylic acids and hydroperoxides via the heterolytic mechanism to form (TPP)(Cl)Cr<sup>V</sup>=O [ $\beta_{\text{LG}} = -0.35$  as seen for heterolysis with (TPP)Fe<sup>III</sup>Cl<sup>6</sup>] and that (TPP)Mn<sup>III</sup>Cl in benzonitrile does not react with hydroperoxides (even the most acidic) due to a very great dependence upon the acidity of YOH ( $\beta_{\text{LG}} = -1.2$ ) but does yield (TPP)(Cl)Mn<sup>V</sup>=O with peroxy-carboxylic acids.<sup>7</sup>

The two reactions of [Porph(X)Fe<sup>IV</sup>=O]<sup>+</sup> species which have received the most attention are "oxygen" insertion into carbon-hydrogen bonds to provide the corresponding alcohol and the epoxidation of alkenes. From stereochemical and isotope distribution studies, there has been proposed, for the hydroxylation reaction, the so-called rebound mechanism of eq 5.<sup>8,9</sup>

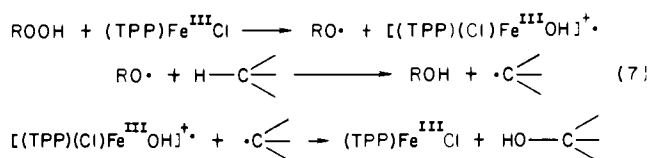


The mechanism for epoxidation of olefins by [(TPP)(X)-Fe<sup>IV</sup>=O]<sup>+</sup> cannot be said to be known. For those [Porph(X)-Fe<sup>IV</sup>=O]<sup>+</sup> species which are substituted at the four meso positions by bulky substituents (as [(TMesP)(X)Fe<sup>IV</sup>=O]<sup>+</sup>), there is a preference in the epoxidation of *cis*- vs. *trans*-1,2-disubstituted

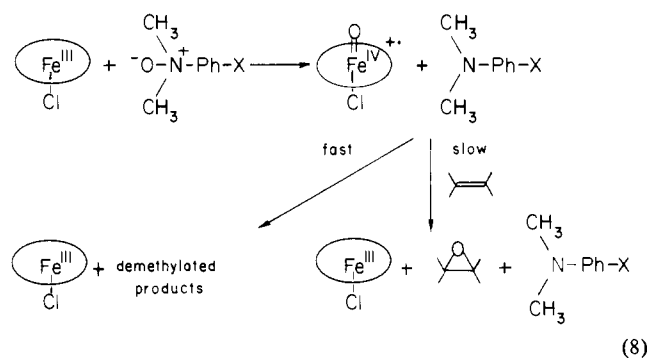
ethenes. That this is not electronic in nature but due to nonbonding repulsion is shown by the observation that PhIO and ferriprotoporphyrin(IX) dimethyl ester provides equal yields of the epoxides of *cis*- and *trans*-stilbene in a competitive experiment.<sup>10</sup> The lack of *cis*-*trans* isomerization accompanying epoxidation, electronic effects, etc., may be interpreted in terms of a concerted oxenoid insertion reaction.<sup>2a,2b,11</sup> The observation, however, of aldehyde products accompanying the epoxidation of styrenes has been suggested as evidence for a carbonium ion intermediate (eq 6).<sup>12</sup>



(Definitive evidence exists for intermediates when (TPP)Mn<sup>III</sup>X species are involved as catalysts for epoxidation.<sup>10</sup>) When aliphatic hydroperoxides are employed as oxygen donors, the products of substrate oxidation have a different distribution than seen with PhI=O or percarboxylic acids.<sup>13,14a</sup> The product distributions obtained from iron(III) and manganese(III) porphyrin-catalyzed oxygenations by alkyl peroxides are greatly affected by the axial ligand.<sup>14b</sup> This observation can be explained through the homolysis of eq 3<sup>5</sup> and the following mechanism, which has been proposed<sup>14</sup> for oxygen insertion into H—C bonds.



We have shown that (TPP)Fe<sup>III</sup>Cl catalyzes oxygen transfer from *N,N*-dimethylaniline *N*-oxide<sup>15</sup> and *p*-cyano-*N,N*-dimethylaniline *N*-oxide (NO)<sup>16</sup> with ensuing demethylation of the resultant *N,N*-dimethylaniline and *p*-cyano-*N,N*-dimethylaniline. Oxygen transfer followed by dealkylation has also been studied with cytochromes P-450<sub>LM2</sub> and P-450<sub>CAM</sub><sup>17</sup> by using NO. Due to the greater ease of demethylation of *N,N*-dimethylaniline, as compared to *p*-cyano-*N,N*-dimethylaniline, by [(TPP)(Cl)-Fe<sup>IV</sup>=O]<sup>+</sup>, the former cannot be employed in epoxidation reactions while the latter can (eq 8). A rather detailed kinetic study



(3) (a) Chin, D.-H.; Balch, A. L.; LaMar, G. N. *J. Am. Chem. Soc.* **1980**, *102*, 1446. (b) Chin, D.-H.; LaMar, G. N.; Balch, A. L. *Ibid.* **1980**, *102*, 5945. (c) LaMar, G. N.; deRopp, J. S.; Lechoslaw, L.-G.; Balch, A. L.; Johnson, R. B.; Smith, K. M.; Parish, D. W.; Cheng, R.-J. *Ibid.* **1983**, *105*, 782. (d) Goff, H. M.; Phillippe, M. A. *Ibid.* **1983**, *105*, 7567. (e) Balch, A. L.; Chan, Y.-W.; Cheng, R.-J.; LaMar, G. N.; Latos-Grazynski, L.; Renner, M. W. *Ibid.* **1984**, *106*, 7779.

(4) Traylor, T. G.; Lee, W. A.; Stynes, D. V. *J. Am. Chem. Soc.* **1984**, *106*, 755.

(5) Lee, W. A.; Bruice, T. C. *J. Am. Chem. Soc.* **1985**, *107*, 513.

(6) Yuan, L.-C.; Bruice, T. C. *J. Am. Chem. Soc.* **1985**, *107*, 512.

(7) Yuan, L.-C.; Bruice, T. C. *Inorg. Chem.* **1985**, *24*, 986.

(8) Groves, J. T.; McClusky, G. A. *J. Am. Chem. Soc.* **1976**, *98*, 859.

(9) Groves, J. T.; Akinbote, O. F.; Avaria, G. E. In "Microsomes, Drug Oxidations, and Chemical Carcinogenesis"; Academic Press: New York, 1980; p 253.

(10) (a) Smegal, J. A.; Hill, C. L. *J. Am. Chem. Soc.* **1983**, *105*, 2920.

(b) Groves, J. T.; Kruper, W. J., Jr.; Haushalter, R. C. *Ibid.* **1980**, *102*, 6377.

(c) Collman, J. P.; Kodadek, T.; Raybuck, S. A.; Meunier, B. *Proc. Natl. Acad. Sci. U.S.A.* **1983**, *80*, 7039. (d) Collman, J. P.; Brauman, J. I.; Meunier, B.; Raybuck, S. A.; Kodadek, T. *Ibid.* **1984**, *81*, 3245. (e) Yuan, L.-C.; Bruice, T. C. *J. Chem. Soc., Chem. Commun.* **1985**, 868.

(11) (a) Groves, J. T.; Nemo, T. E. *J. Am. Chem. Soc.* **1983**, *105*, 5788.

(b) Groves, J. T.; Nemo, T. E. *Ibid.* **1983**, *105*, 6243.

(12) Groves, J. T.; Myers, R. S. *J. Am. Chem. Soc.* **1983**, *105*, 5791.

(13) Gold, A.; Toney, G. E.; Wisnieff, T. J.; Snugaiah, R. *Rev. Biochem. Toxicol.* **1982**, *4*, 31.

of demethylation, hydroxylation, and epoxidation with NO employing various ligated (TPP)Mn<sup>III</sup>X species has recently appeared.<sup>1</sup> Presented in this study is an in-depth kinetic examination of the catalysis of the transfer of "oxygen" from *p*-cyano-*N,N*-dimethylaniline *N*-oxide to (TPP)Fe<sup>III</sup>Cl, which yields *p*-cyano-*N,N*-dimethylaniline (DA) and [(TPP)(Cl)Fe<sup>IV</sup>=O]<sup>+</sup>, and the ensuing multistep reaction of [(TPP)(Cl)Fe<sup>IV</sup>=O]<sup>+</sup> with DA and its oxidation products as well as reaction of [(TPP)(Cl)Fe<sup>IV</sup>=O]<sup>+</sup> with alkenes. By determining the rate constant for the commitment step of "oxygen" transfer from NO to (TPP)Fe<sup>III</sup>Cl, the rate constants for the formation of the various products, and the percent yields of products, it has been possible to calculate by computer simulation the various rate constants (such as those of amine oxidation and epoxidation by [(TPP)(Cl)Fe<sup>IV</sup>=O]<sup>+</sup>).

## Experimental Section

**Physical Measurements.** UV-visible spectra were recorded on a Cary 118C or Perkin-Elmer 553 spectrophotometer. The latter was employed for all kinetic studies and was equipped with a constant temperature cell holder maintained at 25 °C. This spectrophotometer was housed in a glovebox containing an oxygen-free N<sub>2</sub> atmosphere. All spectra were determined in CH<sub>2</sub>Cl<sub>2</sub> (grade A or grade C). HPLC analyses were performed under the following conditions: the apparatus consisted of two Altex 100 dual-stroke pumps equipped with an Altex solvent programmer, an Altex RSILCN analytical column (5 μm, 250 × 4.6 mm), a 5-μm alumina precolumn, a Rheodyne injector with a 100-μL loop, an HP 1040A diode-array UV detector, and two HP 3392A integrators. This system was interfaced to an HP 85B computer and operated by HP software designed for UV measurements. The flow rate was set at 1.2 mL/min, and an exponential solvent gradient with an initial mixture of 9:1 hexane/EtOAc and a final mixture of 1:1 hexane/EtOAc were used (gradient time = 50 min). Each sample was monitored and integrated at two wavelengths: 280 and 320 nm. Injection sizes varied from 25 to 40 μL depending upon the concentration of the solution. Gas chromatographic analyses were performed by using a Varian Model 3700 gas chromatograph equipped with a flame ionization detector, a Varian WCOT capillary column (0.2 mm i.d., 25 m length), and an HP 3392A integrator. Helium was used as the carrier gas.

GC-MS analysis was carried out on an HP 5992A system with a J and W DB-1 methylsilicone bonded phase fused silica WCOT capillary column (0.3 mm i.d., 15 m length). <sup>1</sup>H NMR spectra were recorded on a Nicolet NT-300 spectrometer (300 MHz). Chemical shifts are reported in parts per million (δ) downfield from tetramethylsilane (TMS). Splitting patterns are designated as follows: s, singlet; d, doublet; t, triplet; q, quartet; m, multiplet. High-resolution mass spectra were obtained from a VG micromass ZAB-2F mass spectrometer operating in the electron impact mode at 70 eV. Thin-layer chromatography (TLC) was performed on 0.25- or 1.0-mm neutral alumina-coated glass plates (Analtech). Column chromatography was performed by using neutral alumina (Sigma, grade I). The amount of formaldehyde produced was determined by the method of Nash.<sup>18</sup>

**Materials.** Dichloromethane was purified in the following manner: the reagent grade dichloromethane was washed with concentrated sulfuric acid until the sulfuric layer was colorless, followed by washings with water, 10% Na<sub>2</sub>CO<sub>3</sub>, and water once again. It was dried over calcium chloride and then was distilled from calcium hydride under N<sub>2</sub> and was protected from light by covering the distillation apparatus with aluminum foil. The solvent was then stored in brown bottles over molecular sieves (4 Å) and was degassed with N<sub>2</sub> for 1 h before storing it under a nitrogen atmosphere in the glovebox. Toluene and benzene were purified by distilling them from Na/benzophenone. Tetrahydrofuran was distilled from lithium aluminum hydride. (All were stored in brown bottles over molecular sieves, 4 Å.)

Tetraphenylporphyrin was purchased from Aldrich. 2,3-Dimethyl-2-butene (TME) was purchased from Aldrich (99%+, gold label) and distilled under an inert atmosphere from powdered NaOH (3 times). 2,4,6-Tri-*tert*-butylphenol (TBPH) was purchased from Aldrich and was recrystallized from EtOH/H<sub>2</sub>O. The white crystals were then dried overnight at 100 °C/30 torr. Cyclohexane, diethyl ether, norbornylene,

*trans*-stilbene, *cis*-stilbene, cyclohexene oxide, cyclohexen-3-ol, *trans*-stilbene oxide, and cyclohexanol were purchased from Aldrich and used without further purification. *p*-Cyano-*N,N*-dimethylaniline (DA) and *p*-cyanoaniline (A) were obtained from Aldrich and were recrystallized from ethanol/diethyl ether.

*p*-Cyano-*N,N*-dimethylaniline *N*-oxide (NO) was prepared by the method of Craig and Puroshothman<sup>19</sup> and was recrystallized under a dry N<sub>2</sub> atmosphere from acetone/petroleum ether. *N,N'*-Dimethyl-*N,N'*-bis(*p*-cyanophenyl)hydrazine (H) was prepared according to the method of Ashley.<sup>20</sup> The product was further purified by preparative TLC (hexane/CHCl<sub>3</sub>, 70:30). *N*-Formyl-*p*-cyano-*N*-methylaniline (FA) was prepared by modification of the procedure of Fry.<sup>21</sup> *p*-Cyano-*N*-methylaniline (MA) (0.1 g) and HCOOH (3.0 mL) were added to 10 mL of reagent-grade benzene. The reaction was refluxed overnight by using a Dean-Stark apparatus. Evaporation of the solvent followed by preparative TLC (CHCl<sub>3</sub>/hexane, 30:70) yielded pure product.<sup>22</sup> *p*-Cyano-*N*-methylaniline (MA) was prepared by dropwise addition of 30 mL of 2.81 M MeI (in methanol) to a methanol solution (30 mL) of A (11.35 g, Aldrich) over a 1-h period. The resulting mixture was refluxed for 30 h. The solvent was evaporated in vacuo. The remaining residue was dissolved in chloroform (100 mL) and washed with 1 M NaOH (2 × 50 mL). The organic layer was dried over Na<sub>2</sub>SO<sub>4</sub> followed by evaporation in vacuo. The crude product was purified by column chromatography (alumina, 70:30 hexane/CHCl<sub>3</sub>). The MA was recrystallized from diethyl ether/petroleum ether and gave the proper <sup>1</sup>H NMR and melting point.<sup>23</sup> *N,N'*-Bis(*p*-cyanophenyl)-*N*-methylmethylenediamine (MD) was obtained from HPLC (under the conditions listed in the Physical Measurements section) of the reaction mixture resulting from the (TPP)Fe<sup>III</sup>Cl (10.0 mg) catalyzed decomposition of NO (40.0 mg) and was identified by <sup>1</sup>H NMR and high-resolution mass spectroscopy.<sup>24</sup> *meso*-(Tetraphenylporphinato)iron(III) chloride [(TPP)-Fe<sup>III</sup>Cl] was prepared by the procedure of Alder.<sup>25</sup> The ethyl carbamate of MA was prepared by adding a toluene solution (10 mL) of ethyl chloroformate (2.3 mL, 24.1 mmol dropwise) over a 1-h period to an ice-cooled solution of MA (3.05 g, 23.1 mmol) and 2,6-lutidine (2.6 mL, 22.3 mmol) in toluene. After warming to room temperature, the reaction mixture was stirred for 2 h, washed successively with 1 N HCl, and saturated NaHCO<sub>3</sub> and H<sub>2</sub>O. The organic layer was then dried over Na<sub>2</sub>SO<sub>4</sub> and evaporated in vacuo. The resulting residue gave the following <sup>1</sup>H NMR: δ 1.0 (t, 3 H, *J* = 7 Hz), 2.8 (s, 3 H), 3.7 (q, 2 H, *J* = 7 Hz), 7.0 (m, 4 H). The ethyl carbamate of *p*-cyano-*N*-(trideuteriomethyl)aniline was prepared as described above using *p*-cyano-*N*-(trideuteriomethyl)aniline instead of MA. *p*-Cyano-*N*-(trideuteriomethyl)aniline was prepared by the method stated previously employing the ethyl carbamate of A. The ethyl carbamate of A was prepared from *p*-cyanoaniline (A) by the technique described above. *p*-Cyano-*N*-methyl-*N*-(trideuteriomethyl)aniline was prepared by adding an ethereal solution (15 mL) of the ethyl carbamate of MA (3.33 g, 16.3 mmol) dropwise to an ice-cooled suspension of LiAlD<sub>4</sub> (0.80 g, 19.0 mmol) in Et<sub>2</sub>O (10 mL). The reaction mixture was stirred for 1 h (under a N<sub>2</sub> atmosphere). After warming to room temperature, it was stirred an additional 1.5 h. The reaction mixture is then refluxed for 1 h, cooled in an ice-bath, and quenched by the addition of 10% NaOH. The resulting solid was removed by filtration and the filtrate dried over K<sub>2</sub>CO<sub>3</sub>. Fractional distillation yielded a clear oil (bp 194–195 °C) which gave the following <sup>1</sup>H NMR: δ 2.8 (s, 3 H), 6.8 (m, 2 H), 7.2 (m, 2 H). *p*-Cyano-*N,N*-bis(trideuteriomethyl)aniline was prepared as above, except by using the ethyl carbamate of *p*-cyano-*N*-(trideuteriomethyl)aniline. The *N*-oxides of the deuterated anilines were prepared by the method of Craig and Puroshothman.<sup>19</sup> Cyclohexene was washed with 1 M NaOH, dried with anhydrous MgSO<sub>4</sub>, refluxed over freshly powdered NaOH (2 h), and distilled (bp 81–82 °C) before use. *cis*-Stilbene oxide and norbornylene oxide were prepared by the method of Pasto and Cumbo.<sup>26</sup>

**Kinetics.** To a known amount of (TPP)Fe<sup>III</sup>Cl in CH<sub>2</sub>Cl<sub>2</sub> was added a CH<sub>2</sub>Cl<sub>2</sub> solution of NO. The kinetic run was initiated (*t* = 0) upon mixing of the temperature-equilibrated (25 °C) NO and (TPP)Fe<sup>III</sup>Cl. The reaction was monitored spectrophotometrically at 320 nm for at least 9 × *t*<sub>1/2</sub>. For those reactions involving the addition of TME, DA, MA,

(19) Craig, J. C.; Puroshothman, K. K. *J. Org. Chem.* **1970**, *35*, 1721.

(20) Ashley, J. N.; Berg, S. S. *J. Chem. Soc.* **1957**, 3089.

(21) Fry, D. J.; Kendall, J. D.; Morgan, A. J. *J. Chem. Soc.* **1960**, 5062.

(22) <sup>1</sup>H NMR: δ 3.35 (s, 3 H), 7.28 (d, 2 H), 7.73 (d, 1 H), 8.66 (s, 1 H).

(23) Kadin, S. B. *J. Org. Chem.* **1973**, *38*, 1348.

(24) <sup>1</sup>H NMR: δ 3.23 (s, 3 H), 4.12 (d, 2 H), 6.66 (m, 4 H), 7.40 (m, 4 H). The high-resolution mass spectrum showed the molecular formula to be C<sub>16</sub>H<sub>14</sub>N<sub>4</sub> 262.1232 (calcd for C<sub>16</sub>H<sub>14</sub>N<sub>4</sub> 262.1334).

(25) Alder, A. D.; Largo, F. R.; Varadi, V. *Inorg. Synth.* **1976**, *16*, 213.

(26) Pasto, D. J.; Cumbo, C. C. *J. Org. Chem.* **1965**, *30*, 1271.

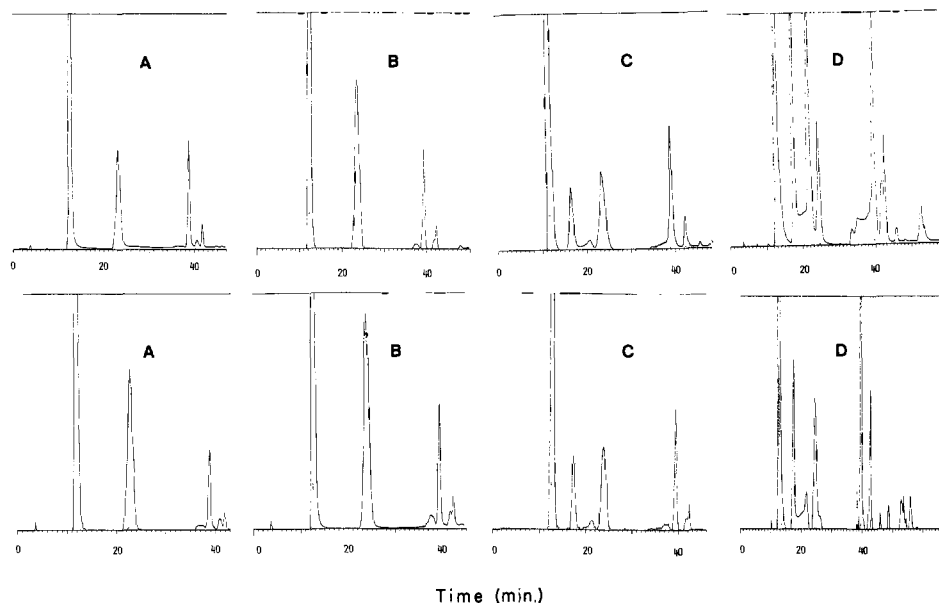
(14) (a) Mansuy, D.; Bartoli, J. F.; Momenteau, M. *Tetrahedron Lett.* **1982**, *23*, 2781. (b) Mansuy, D.; Battinoi, P.; Renaud, J.-P. *J. Chem. Soc., Chem. Commun.* **1984**, 1255.

(15) Shannon, P.; Bruice, T. C. *J. Am. Chem. Soc.* **1981**, *103*, 4580.

(16) Nee, M. W.; Bruice, T. C. *J. Am. Chem. Soc.* **1982**, *104*, 6123.

(17) Heimbrook, D. C.; Murray, R. I.; Egeberg, E. D.; Sligar, S. G.; Nee, M. W.; Bruice, T. C. *J. Am. Chem. Soc.* **1984**, *106*, 1514.

(18) Nash, T. *Biochem. J.* **1953**, *55*, 416.



**Figure 1.** HPLC elution patterns of NO/(TPP)Fe<sup>III</sup>Cl reaction mixtures showing the effect of the CH<sub>2</sub>Cl<sub>2</sub> solvent purity on the number of products obtained from the reaction. (A) An extensively purified CH<sub>2</sub>Cl<sub>2</sub> (see Materials section) stored under N<sub>2</sub> away from light and passed through an oven-baked (150 °C, in vacuo) neutral alumina column under a N<sub>2</sub> atmosphere just prior to initiation of the reaction was used. (B) The CH<sub>2</sub>Cl<sub>2</sub> was purified and stored in the same manner as in A but was not passed through alumina before use. (C) The solvent used was Aldrich Gold Label CH<sub>2</sub>Cl<sub>2</sub>. (D) Solvent grade CH<sub>2</sub>Cl<sub>2</sub> was employed in the reaction.

**Table I.** Product Yield for the Six Known Compounds When Solvents of Different Purity Are Employed in the (TPP)Fe<sup>III</sup>Cl-Catalyzed Decomposition of NO under Aerobic Conditions

([NO]<sub>i</sub> = 2.7 × 10<sup>-3</sup> M, [(TPP)Fe<sup>III</sup>Cl]<sub>i</sub> = 7.8 × 10<sup>-5</sup> M)

prod	solv grade % yield			
	A	B	C	D
DA	57	59	57	53
MA	26	26	11	8
A	2	2	3	3
H	10	7	10	8
FA	3	5	4	5
MD	6	6	6	6

**Table II.** Effect of Solvent Purity on the Kinetics Determined at 320 nm

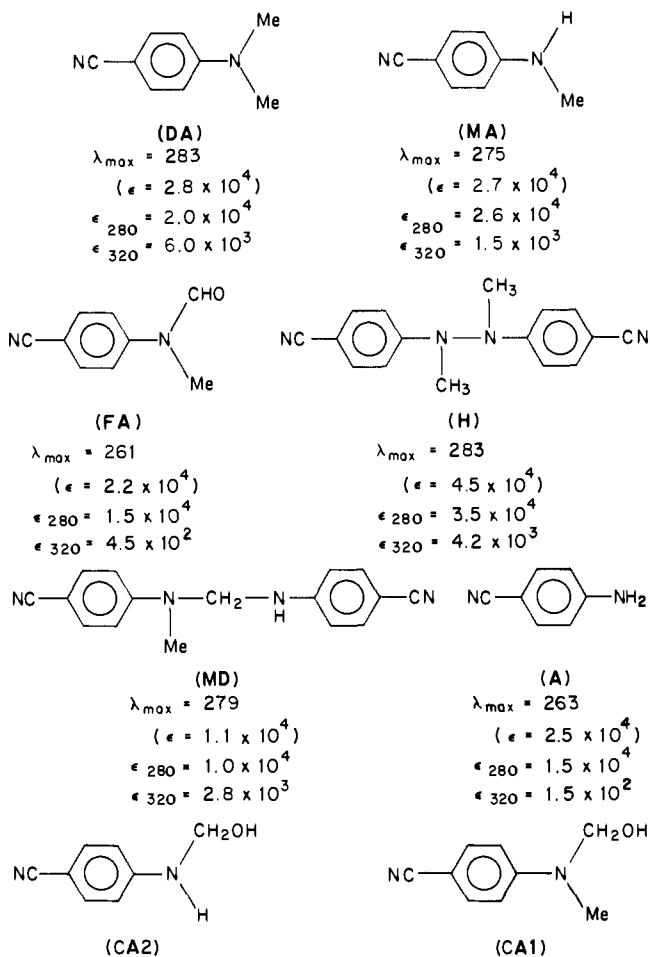
solv	[(TPP)Fe <sup>III</sup> Cl] <sub>i</sub> , M	[NO] <sub>i</sub> , M	k <sub>42</sub> , s <sup>-1</sup>
A	7.8 × 10 <sup>-5</sup>	2.7 × 10 <sup>-3</sup>	3.1 × 10 <sup>-4</sup>
B	7.8 × 10 <sup>-5</sup>	2.5 × 10 <sup>-3</sup>	3.4 × 10 <sup>-4</sup>
C	7.4 × 10 <sup>-5</sup>	2.6 × 10 <sup>-3</sup>	3.2 × 10 <sup>-4</sup>
D	8.1 × 10 <sup>-5</sup>	2.3 × 10 <sup>-3</sup>	3.2 × 10 <sup>-4</sup>

H, FA, or A to the reaction mixture, a solution of NO in CH<sub>2</sub>Cl<sub>2</sub> was added to a CH<sub>2</sub>Cl<sub>2</sub> solution of the (TPP)Fe<sup>III</sup>Cl and one of the compounds listed above. The kinetic run was initiated and monitored in the same manner as stated above. For those runs where the time courses for the formation of DA, MA, H, FA, A, MD, and CH<sub>2</sub>O were determined, aliquots were withdrawn under flowing argon or nitrogen (from an apparatus that was maintained at 25 °C) with a syringe and transferred to dry ice-chilled gas-tight nitrogen-filled vials. The samples were kept in dry ice until analysis by HPLC under the conditions listed in the Physical Measurements section. In the case of the "trap" experiments involving TBPH, the NO (in CH<sub>2</sub>Cl<sub>2</sub>) was added to a CH<sub>2</sub>Cl<sub>2</sub> solution of the iron(III) porphyrin and TBPH, to initiate the kinetic run. The reaction was monitored spectrophotometrically at 630 nm for at least 9 × t<sub>1/2</sub>. Upon completion of the reactions, the solutions were analyzed by HPLC and GC. The concentrations of the products were determined from standard curves prepared from the known compounds.

Calculations were performed on an HP 9825A calculator equipped with an HP 9864A digitizer and HP 9867A plotter. Reaction scheme simulations were carried out by using an HP 9816 personal computer as a smart terminal to a Digital VAX 11/750 computer equipped with a Gear based software made available by Dr. Paul Meakin of DuPont Central Research.

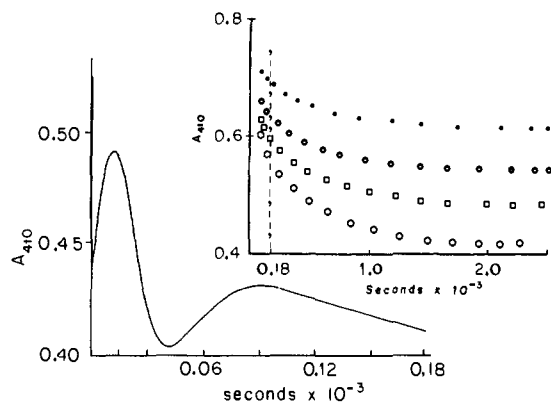
*The purity of the dichloromethane solvent determines the complexity*

**Chart I**

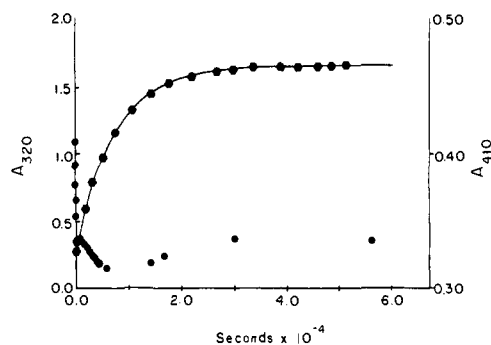


the carbinolamines CA1 and CA2 are required intermediates but have not been isolated

of the reaction of NO and (TPP)Fe<sup>III</sup>Cl. This result is evidenced by the increase in the number of separable aromatic products as the solvent purity decreases. Solvent purity is indicated by the letters A to D. Grade



**Figure 2.** Changes in the magnitude of the Soret band ( $A_{410}$ ) during the initial portion of the (TPP)Fe<sup>III</sup>Cl-catalyzed decomposition of NO. The exponential decrease in  $A_{410}$  that occurs during the remainder of the reaction is shown in the inset.



**Figure 3.** Comparison of the time course for  $A_{410}$  and  $A_{320}$ , illustrating the fact that the decrease in  $A_{410}$  leveled off at about one half-life for the appearance of products ( $A_{320}$ ).

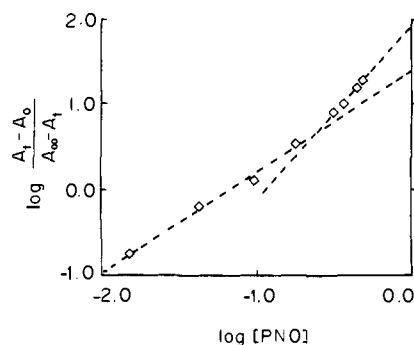
A solvent represents an extensively purified product (see Materials section) stored under  $N_2$  away from light and passed through an oven baked ( $150^\circ C$ , in vacuo) neutral alumina column under a  $N_2$  atmosphere just prior to initiation of a reaction. Grade B solvent is purified (and stored) in the same manner as grade A solvent but is not passed through alumina before use. Grade C dichloromethane represents Aldrich Gold Label, and grade D dichloromethane is simply solvent grade.

The decomposition of NO ( $5.0 \times 10^{-4}$  to  $1.7 \times 10^{-2}$  M) in the presence of (TPP)Fe<sup>III</sup>Cl ( $4.6 \times 10^{-5}$  to  $8.0 \times 10^{-5}$  M) was carried to completion in solvents A through D. The products were separated by HPLC. Examples of integrated elution diagrams for the reactions carried out in solvents A–D are shown in Figure 1. As evidenced, the better the quality of the solvent, the cleaner the reaction; i.e., fewer aromatic products are detected when using grade A solvent than when employing grade D solvent in the reactions. This result holds true for reactions carried out in the presence of air as well as under an  $O_2$ -free nitrogen atmosphere (see Figure 1).

For the run in grade A solvent, six products are formed, and these have been characterized as DA, MA, A, H, FA, and MD (respective elution times: 12, 23, 36, 39, 40.5, and 42 min). This same product analysis is observed for the reaction run in grade B solvent (see Figure 1). However, when one uses grade C methylene chloride, three unidentified products are formed in addition to the six compounds listed above (elution times of new compounds: 16.5, 20.5, and 35 min). The elution pattern becomes even more complicated when grade D solvent is employed in the reaction, i.e., 4 additional compounds are also observed (elution times: 49, 53, 54, and 56 min), giving a total of 13 appreciable products (>1% yield each).

Table I shows that the percent yield for each of the six known products is the same for reactions run when using grade A or grade B solvents, while when grade C and grade D solvents are employed the difference in product yield is only evidenced for MA (i.e., from ~25% for A and B to ~10% for C and D). This result suggests that the additional products seen with grade C and D solvents are due to the oxidation of MA or result from a process that competes with the formation of MA.

Finally, the solvent purity does not affect the rates of product formation. Thus, the same pseudo-first-order rate constant was obtained from the exponential increase in  $A_{320}$  with time in the various grades of  $CH_2Cl_2$  (Table II). Even though no difference is observed in the



**Figure 4.** Plot of  $\log (A_t - A_0)/(A_\infty - A_t)$  vs.  $\log [PNO]$  where the slope of each line determines the stoichiometry of the PNO/(TPP)Fe<sup>III</sup>Cl complex that is formed. The equilibrium constants  $K_1$  and  $\beta_2$  were obtained by extrapolation of the respective slopes of their  $y$  intercept.

(TPP)Fe<sup>III</sup>Cl-catalyzed decomposition of NO with either grade A or grade B solvent, the grade A methylene chloride was employed throughout this study to allow comparison of results to those obtained (work in progress) with the  $SbF_6^-$  and  $ClO_4^-$  ligand iron(III) tetraphenylporphyrins. With these weakly ligated porphyrins, experimental observations are altered when reactions are transferred from grade A to grade B solvent.

As stated earlier, neither the products nor their yields are altered by the presence or absence of oxygen. Comparison of the kinetic results obtained in the presence and absence of oxygen are limited. However, from what comparisons were made, it would appear as though the presence of  $O_2$  has no effect upon the kinetics of the reaction. Nevertheless, the studies described herein were carried out (unless stated otherwise) under an inert atmosphere. This was done so that no question could be raised at a future date concerning any possible  $O_2$  involvement and to allow for an absolutely dry atmosphere, since NO is hygroscopic.

## Results

The objective of this investigation has been to determine the important details of the reaction of *p*-cyano-*N,N*-dimethylaniline *N*-oxide (NO) with *meso*-(tetraphenylporphinato)iron(III) chloride [(TPP)Fe<sup>III</sup>Cl] in the absence and presence of added hydrocarbon substrate. The products formed on decomposition of NO in the presence of (TPP)Fe<sup>III</sup>Cl are shown in Chart I (Experimental Section).

The influence of solvent purity and admittance of  $O_2$  to the reaction solutions upon products formed and the kinetics of the reaction are considered in the Experimental Section. The experiments described in this section were carried out in a highly purified  $CH_2Cl_2$  solvent (referred to in the Experimental Section as grade A) at  $25^\circ C$  under a  $N_2$  atmosphere. In what follows there will be described the following: (i) changes in the Soret absorbance of (TPP)Fe<sup>III</sup>Cl during the course of its multiple turnovers in catalysis of the decomposition of the *N*-oxide. Changes of ligation of the Fe<sup>III</sup> moiety are reflected in the Soret region at  $A_{410}$ ; (ii) the determination of the equilibrium constants for complexation of picoline *N*-oxide and (TPP)Fe<sup>III</sup>Cl as a possible means to ascertain what is reasonably expected for complexation of NO by (TPP)Fe<sup>III</sup>Cl; (iii) kinetic studies at  $A_{320}$  which determine the molecularity of the reaction in NO and (TPP)Fe<sup>III</sup>Cl, the dynamics for the formation of individual products, the stability of the (TPP)Fe<sup>III</sup>Cl catalyst to multiple turnovers of NO and the ability of each product to serve as substrate; (iv) the determination that the commitment step for NO turnover is oxygen transfer from NO to the iron moiety of (TPP)Fe<sup>III</sup>Cl and that the various products of NO decomposition are formed by reaction of the resultant higher valent iron oxoporphyrin species with the *p*-cyano-*N,N*-dimethylaniline (DA); (v) studies of the oxidation of hydrocarbons by NO which show that these oxidations result from competition of the hydrocarbon with DA for the higher valent iron oxoporphyrin species.

Changes in the Soret band of (TPP)Fe<sup>III</sup>Cl at 410 nm can be studied over a wide range of concentrations of NO since the latter and its products of decomposition have very little absorbance at this wavelength. The changes in  $A_{410}$  during the initial portion

**Table III.** Percentage Yields of Products (Determined by HPLC at 280 and 320 nm) and Their Contribution to the Absorbance at 320 nm for the Decomposition of NO in the Presence of (TPP)Fe<sup>III</sup>Cl

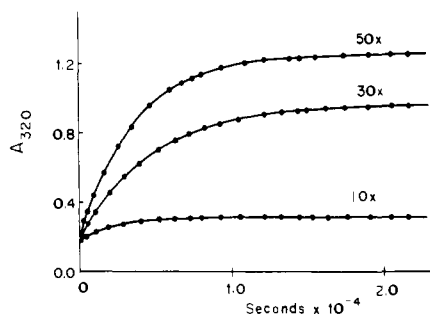
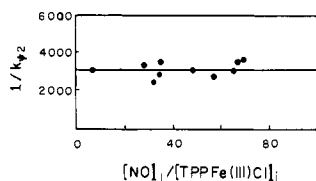
reactants			% yields ( $A_{320}$ )							$\Sigma\%$ yields	$\Sigma A_{320}$	( $A_{320}$ exptl)
$[(\text{TPP})\text{Fe}^{\text{III}}\text{Cl}]_i$	$[\text{NO}]_i$	anaerobic	DA	MA	H	A	FA	MD				
$7.5 \times 10^{-5}$	$5.0 \times 10^{-3}$	yes	60 (1.56)	25 (0.15)	12 (0.12)	2	4	6 (0.17)	109	2.00	1.86	
$7.9 \times 10^{-5}$	$4.3 \times 10^{-3}$	yes	54 (1.38)	25 (0.12)	11 (0.11)	4	5	7 (0.12)	106	1.73	1.62	
$7.8 \times 10^{-5}$	$5.1 \times 10^{-3}$	yes	53 (1.44)	35 (0.23)	12 (0.12)	2	4	6 (0.12)	112	1.91	1.81	
$7.5 \times 10^{-5}$	$2.6 \times 10^{-3}$	no	57 (0.78)	26 (0.17)	10 (0.03)	2	3	6 (0.05)	104	1.03	1.16	
$7.5 \times 10^{-5}$	$3.0 \times 10^{-3}$	no	53 (0.84)	33 (0.15)	13 (0.04)	2	4	6 (0.10)	111	1.13	1.05	
$7.1 \times 10^{-5}$	$3.9 \times 10^{-3}$	no	52 (1.08)	29 (0.16)	12 (0.05)	2	4	8 (0.13)	107	1.42	1.42	
$7.4 \times 10^{-5}$	$5.1 \times 10^{-3}$	no	56 (1.50)	29 (0.22)	12 (0.07)	2	5	6 (0.10)	110	1.89	1.72	

**Table IV.** Effect of  $[(\text{TPP})\text{Fe}^{\text{III}}\text{Cl}]_i$  on the Kinetics and the Product Ratios of the Catalyzed Decompositions of NO ( $3 \times 10^{-3}$  M)

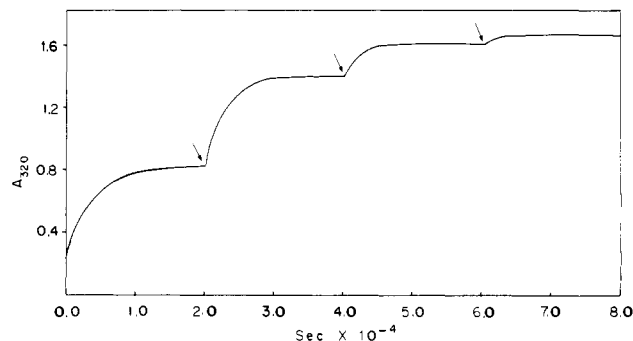
$[(\text{TPP})\text{Fe}^{\text{III}}\text{Cl}]_i$ , M	turnover no.	$k_{\psi 2}$ , s <sup>-1</sup>	% yields						total % yield
			DA	MA	H	FA	A	MD	
$5.0 \times 10^{-4}$	6	$1.5 \times 10^{-3}$	70	7	9	6	3	8	103
$2.5 \times 10^{-4}$	12	$7.5 \times 10^{-4}$	67	14	9	4	2	7	103
$1.2 \times 10^{-4}$	25	$4.0 \times 10^{-4}$	58	17	11	6	3	7	102
$6.2 \times 10^{-5}$	50	$2.3 \times 10^{-4}$	56	22	8	3	2	6	97
$3.1 \times 10^{-5}$	100	$1.6 \times 10^{-4}$	56	23	7	4	3	7	100

**Table V.** Product Concentrations from the Repetitive Addition of NO in the (TPP)Fe<sup>III</sup>Cl-Catalyzed Decomposition of NO: Concentration of Products Formed (Absorbance due to Compound) [% Yields based upon Total NO Consumed]

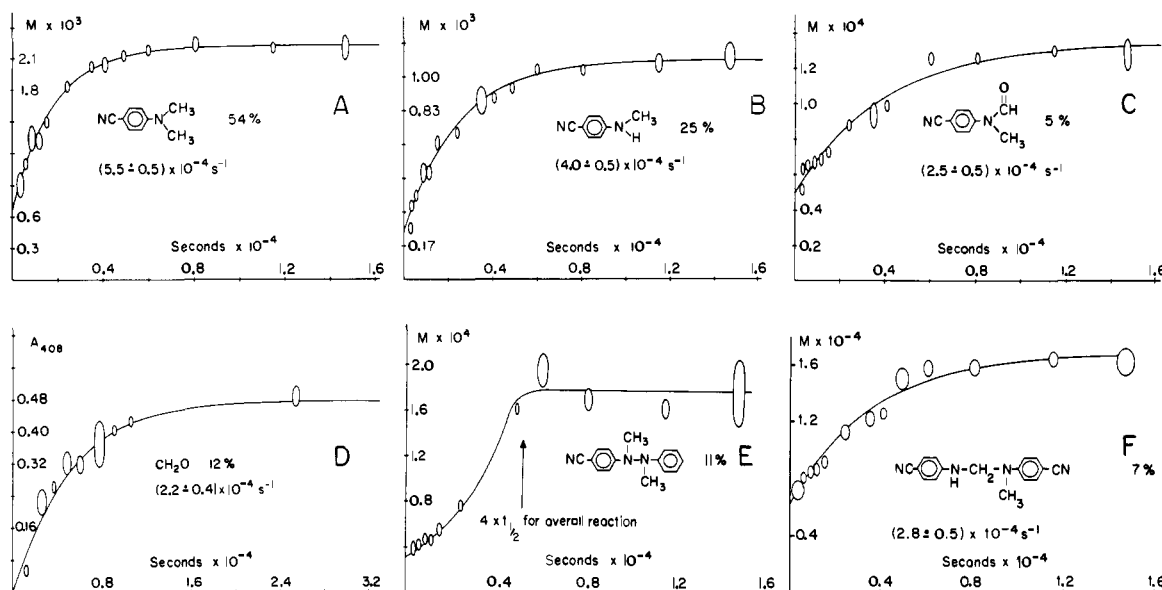
prod	aliquot ( $[\text{NO}]_i$ , M)			
	1st ( $2.0 \times 10^{-3}$ M)	2nd ( $4.0 \times 10^{-3}$ M)	3rd ( $6.0 \times 10^{-3}$ M)	4th ( $8.0 \times 10^{-3}$ M)
DA	$1.1 \times 10^{-3}$ (0.55) [55]	$2.2 \times 10^{-3}$ (1.10) [55]	$2.8 \times 10^{-3}$ (1.40) [47]	$3.1 \times 10^{-3}$ (1.55) [39]
MA	$3.5 \times 10^{-4}$ (0.09) [18]	$5.1 \times 10^{-4}$ (0.14) [13]	$1.0 \times 10^{-3}$ (0.20) [17]	$1.6 \times 10^{-3}$ (0.21) [20]
H	$1.1 \times 10^{-4}$ (0.07) [11]	$2.3 \times 10^{-4}$ (0.11) [12]	$4.4 \times 10^{-4}$ (0.11) [15]	$4.2 \times 10^{-4}$ (0.15) [11]
FA	$4.6 \times 10^{-5}$ [2]	$7.3 \times 10^{-5}$ [2]	$6.8 \times 10^{-5}$ [1]	$6.9 \times 10^{-5}$ [2]
A	$4.6 \times 10^{-5}$ [2]	$8.1 \times 10^{-5}$ [2]	$8.5 \times 10^{-5}$ [2]	$1.2 \times 10^{-4}$ [1]
MD	$8.7 \times 10^{-5}$ (0.06) [9]	$1.5 \times 10^{-4}$ (0.10) [8]	$1.8 \times 10^{-4}$ (0.14) [6]	$1.9 \times 10^{-4}$ (0.15) [5]
$A_{320}$ exptl	0.83	1.43	1.64	1.71
$A_{320}$ calcd	0.79	1.45	1.85	2.06

**Figure 5.** Plot of  $A_{320}$  vs. time for the (TPP)Fe<sup>III</sup>Cl-catalyzed decomposition of NO (where the  $[(\text{TPP})\text{Fe}^{\text{III}}\text{Cl}]_i = 7.5 \times 10^{-5}$  M, and the  $[\text{NO}]_i$  was varied from  $7.5 \times 10^{-4}$  to  $3.8 \times 10^{-3}$  M) showing that the initial rates are dependent on  $[\text{NO}]_i$  but that  $k_{\psi 2}$  is independent of  $[\text{NO}]_i$ .**Figure 6.** Plot of  $1/k_{\psi 2}$  vs.  $[\text{NO}]_i / [(\text{TPP})\text{Fe}^{\text{III}}\text{Cl}]_i$  that illustrates that  $k_{\psi 2}$  is independent of the turnover number.

of the reaction are complex. A plot of  $A_{410}$  vs. time during the first 180 s after mixing ( $[\text{NO}]_i = 5.4 \times 10^{-3}$  M) is shown in the main body of Figure 2. The exponential decrease in  $A_{410}$  which ensues after the first 90 s is shown in the inset of Figure 2 for several NO concentrations ( $1.5 \times 10^{-3}$  to  $1.5 \times 10^{-2}$  M). It should be noted that these changes in  $A_{410}$  with time are not accompanied by the formation of new absorption bands in the Soret region. The behavior of  $A_{410}$  observed in the first 90 s ( $\sim 1/20$  of  $t_{1/2}$  for the

**Figure 7.** Ability of the porphyrin to remain intact under the reaction conditions shown from the kinetics of the (TPP)Fe<sup>III</sup>Cl-catalyzed decomposition of NO where an arrow indicates the introduction of an additional 30 equiv of NO to the reaction mixture ( $[(\text{TPP})\text{Fe}^{\text{III}}\text{Cl}]_i = 8.2 \times 10^{-5}$  M and  $[\text{NO}]_i = 2.0 \times 10^{-3}$  M).

decomposition of NO) will be shown to be due to oscillations in the concentration of the iron(III) porphyrin *N*-oxide complex (see Discussion section) which occur at the onset of the reaction. The greater the  $[\text{NO}]_i$ , the larger is the exponential decrease in  $A_{410}$  observed after 90 s. The rate constant  $k_{\psi 1}$  for this decrease is independent of  $[\text{NO}]_i$  ( $(2.1 \pm 0.1) \times 10^{-3}$  s<sup>-1</sup>). Thus, with an increase in  $[\text{NO}]_i$ , both the decrease of the Soret band (after the first 90 s) and increase in product concentration (vide infra) become larger. The two unequal pseudo-first-order rate constants associated with these absorbance changes ( $k_{\psi 1}$  and  $k_{\psi 2}$ ) are, however, independent of  $[\text{NO}]_i$  (vide infra). The leveling off of the decrease in  $A_{410}$  occurs at about one half-life for the appearance of products (see Figure 3). Finally, after the leveling off of the  $A_{410}$  occurs, a slight increase takes place which is due to the absorbance of the products that are being built up in the decomposition of NO. This increase in  $A_{410}$  is scarcely noticeable at the



**Figure 8.** Time course for each product in the (TPP)Fe<sup>III</sup>Cl ( $7.9 \times 10^{-5}$  M) catalyzed decomposition of NO ( $4.3 \times 10^{-3}$  M) determined by HPLC analysis: (A) *p*-cyano-*N,N*-dimethylaniline, (B) *p*-cyano-*N*-methylaniline, (C) *N*-formyl-*p*-cyano-*N*-methylaniline, (D) formaldehyde, (E) *N,N'*-di-methyl-*N,N'*-bis(*p*-cyanophenyl)hydrazine, (F) *N,N'*-bis(*p*-cyanophenyl)-*N*-methylmethylenediamine.

**Table VI.** Comparison of the First-Order Rate Constants for Product Formation and Increase in  $A_{320}$  from a Reaction Solution Containing Initially [NO] =  $4.3 \times 10^{-3}$  M and [(TPP)Fe<sup>III</sup>Cl] =  $7.9 \times 10^{-5}$  M

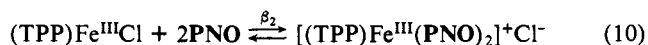
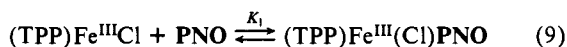
	rate const, s <sup>-1</sup>		rate const, s <sup>-1</sup>
$A_{320}$ with time ( $k_{\psi_2}$ )	$4.4 \times 10^{-4}$	[FA] with time	$2.5 \times 10^{-4}$
[DA] with time	$5.5 \times 10^{-4}$	[MD] with time	$2.8 \times 10^{-4}$
[MA] with time	$4.0 \times 10^{-4}$	[CH <sub>2</sub> O] with time	$2.2 \times 10^{-4}$

**Table VII.** Effect of [TBPH]<sub>i</sub> on the Rate of Formation of the Phenoxy Radical and the Product Yields in the Decomposition of NO ([NO]<sub>i</sub> =  $2.6 \times 10^{-3}$  M) by (TPP)Fe<sup>III</sup>Cl

[TBPH] <sub>i</sub> , M	[(TPP)Fe <sup>III</sup> Cl] <sub>i</sub> , M	$k_{\psi_2}$ , s <sup>-1</sup>	% DA	% MA
0.20	$5.0 \times 10^{-5}$	$4.6 \times 10^{-4}$	100	1
0.15	$1.0 \times 10^{-4}$	$6.0 \times 10^{-4}$	100	1
0.15	$1.0 \times 10^{-4}$	$6.1 \times 10^{-4}$	105	1
0.10	$5.0 \times 10^{-5}$	$3.5 \times 10^{-4}$	104	2
0.02	$5.0 \times 10^{-5}$	$4.1 \times 10^{-4}$	104	2

concentrations of NO used in the kinetic studies of product formation (vide infra). Spectral scans, on completion of the reaction, show that the absorbance of products impinge upon the spectrum of the iron(III) porphyrin as [NO]<sub>i</sub> is increased. The only other change seen in the spectrum of spent reaction solutions was the appearance of a small amount of the  $\mu$ -oxo dimer [(TPP)Fe<sup>III</sup>]<sub>2</sub>O at 571 and 610 nm (its  $\alpha$ ,  $\beta$  bands). The formation of [(TPP)Fe<sup>III</sup>]<sub>2</sub>O is due to reaction of (TPP)Fe<sup>III</sup>Cl with H<sub>2</sub>O produced during the course of the reaction of (TPP)Fe<sup>III</sup>Cl with NO.

*Equilibrium constants for the addition of an N-oxide to (TPP)Fe<sup>III</sup>Cl* were determined by the visible spectral techniques described by Walker et al.<sup>27</sup> For this purpose, picoline *N*-oxide (PNO) was employed since it is unable to transfer its oxygen to (TPP)Fe<sup>III</sup>Cl. The equilibrium binding of PNO was followed at 530 nm where an  $\alpha$ ,  $\beta$  absorbance band appears upon complexation to PNO to (TPP)Fe<sup>III</sup>Cl. The equilibria considered are those of eq 9 and 10. In Figure 4, there is plotted  $\log(A_t - A_0)/(A_\infty -$



$A_t$ ) vs.  $\log[PNO]$  (where  $A_t$  = the absorbance at 530 nm,  $A_0$  =  $A_{530}$  due to (TPP)Fe<sup>III</sup>Cl in the absence of PNO, and  $A_\infty$  = its

absorbance at 530 nm in the presence of a large excess of PNO) where the slopes of plots of this type provide the stoichiometry of the complexes that are formed.<sup>27</sup> The equilibrium constants  $K_1$  ( $18 M^{-1}$ ) and  $\beta_2$  ( $79 M^{-2}$ ) were obtained by extrapolation of the slopes of the  $y$  intercept.

*The time course for the appearance of products in the reaction of NO with (TPP)Fe<sup>III</sup>Cl can be conveniently monitored at 320 nm by spectral observation and by HPLC.* At this wavelength, the absorbance by the metalloporphyrin is minimal. The increase in  $A_{320}$  is due mainly to the formation of DA while H, MA, and MD also contribute. Indeed the summation of the integrated HPLC peak intensities of products determined at 320 nm at completion of the reactions accounts for the absorbance of the reaction solution seen spectrophotometrically at 320 nm (see Table III). As an example of the computations leading to the data in Table III, a sample calculation is considered. When a 0.1 cm path length silica cuvette was used, the absorbance of a solution containing initially  $4.3 \times 10^{-3}$  M NO and  $7.9 \times 10^{-5}$  M (TPP)Fe<sup>III</sup>Cl was 1.62 at time =  $1.5 \times 10^4$  s. HPLC analysis at 320 nm established the solution to be  $2.3 \times 10^{-3}$  M in the major component, DA. When an extinction coefficient of  $6 \times 10^3 M^{-1} cm^{-1}$  for DA at 320 nm is employed, its contribution to the absorbance of the reaction solution is calculated as 1.38. Using this value along with the integrated areas for the other products at 320 nm, there is then calculated the absorbance contribution of each product to the reaction solution. Examination of Table III shows that the spectrally observed  $A_{320}$  of the reaction solution is satisfactorily accounted for by the HPLC determined product compositions. Also, it is seen that DA accounts for 75% of the absorbance at 320 nm; this product is the result of oxygen transfer from NO to iron(III) porphyrin.

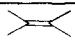

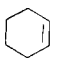
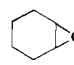
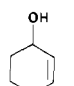
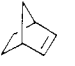
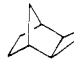
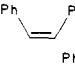
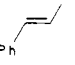
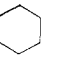
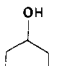
*HPLC analysis of the reaction mixture at 280 and 320 nm gives complete material balance* (Table III). Standard curves were prepared for each product and used in the determination of reaction composition. The standard curves were checked periodically to ensure that the column eluting ability was not changing and, thus, that the standards were accurate. In general, analyses were carried out at 280 nm. However, due to the high concentration of DA and its high extinction coefficient at 280 nm, the percent yield of DA was calculated from the HPLC analysis at 320 nm. On examination of Table III, one notices that the percent yields of products are the same regardless of whether the reactions were carried out under anaerobic or aerobic conditions. However, no

(27) Walker, F. A.; Lo, M.-W.; Ree, M. T. *J. Am. Chem. Soc.* **1976**, *98*, 5552.

**Table VIII.** Kinetic Data from the (TPP)Fe<sup>III</sup>Cl (7.6 × 10<sup>-5</sup> M) Catalyzed Decomposition of NO in the Presence of the Various Oxidation Products, Each at 1.0 × 10<sup>-3</sup> M, and the Influence of These Oxidation Products upon the Percent Yields Derived from NO

oxidat prod	[NO] <sub>0</sub> , M	k <sub>ψ2</sub> , s <sup>-1</sup>	% yields of prod					
			DA	MA	H	FA	A	MD
	2.6 × 10 <sup>-3</sup>	3.5 × 10 <sup>-4</sup>	57	22	8	5	4	8
DA	2.6 × 10 <sup>-3</sup>	2.3 × 10 <sup>-4</sup>	65	22	12	5	2	6
MA	2.6 × 10 <sup>-3</sup>	3.4 × 10 <sup>-4</sup>	70	24	37	2	3	23
H	2.6 × 10 <sup>-3</sup>	3.4 × 10 <sup>-4</sup>	57	22	0	3	4	7
FA	2.6 × 10 <sup>-3</sup>	2.8 × 10 <sup>-4</sup>	57	21	10	6	2	7
A	2.6 × 10 <sup>-3</sup>	1.3 × 10 <sup>-4</sup>	52	43	0	0	0	0

**Table IX.** Oxidation of Alkenes and Alkanes by NO Catalyzed by (TPP)Fe<sup>III</sup>Cl<sup>a</sup>

substrate	prod	yield, <sup>b</sup> %
		90 (89)
		45 (48, 55)
		11 (13, 15)
		36
	<i>cis</i> -stilbene oxide	29 (52, 82)
	<i>trans</i> -stilbene oxide	17 (2, trace)
		2 (8)

<sup>a</sup> The ratio of substrate to NO to (TPP)Fe<sup>III</sup>Cl in the reactions was 100:1.0:1. <sup>b</sup> GC yields based on NO added. Yields with iodobenzene and (TPP)Fe<sup>III</sup>Cl are given in parentheses.

further experiments were carried out in the presence of O<sub>2</sub>. In the reactions of Table III, [(TPP)Fe<sup>III</sup>Cl]<sub>0</sub> is essentially constant and NO does not vary greatly.

**Dependence of the Rate Constant upon the Concentration of Reactants.** At constant [(TPP)Fe<sup>III</sup>Cl]<sub>0</sub>, the apparent-first-order rate constant, k<sub>ψ2</sub>, calculated from the change in absorbance at 320 nm for product formation, does not vary appreciably with changes in [NO]<sub>0</sub> (see Figures 5 and 6). This observation goes hand in hand with the increase in initial rates on increase in [NO]<sub>0</sub> (see Figure 5) and shows that the (TPP)Fe<sup>III</sup>Cl catalyst is not saturated with the *N*-oxide at the concentrations of NO used in these studies. As anticipated, k<sub>ψ2</sub> is a linear function of [(TPP)Fe<sup>III</sup>Cl]<sub>0</sub> (Table IV). Thus, the (TPP)Fe<sup>III</sup>Cl-catalyzed decomposition of NO is first-order in iron(III) porphyrin and in *N*-oxide. The average value of k<sub>ψ2</sub>/[(TPP)Fe<sup>III</sup>Cl]<sub>0</sub> provides the second-order rate constant of (4 ± 2) M<sup>-1</sup> s<sup>-1</sup>.

Finally, the product yields (determined by HPLC analysis) vary little with the initial iron(III) porphyrin concentration for reactions which involve between 10 (Table IV) and 90 turnovers of NO. There is a very small change in the ratio of DA:MA for less than 10 turnovers (see Table IV) and an equally small difference for greater than 90 turnovers (vide infra, Table V).

A knowledge of the stability of the (TPP)Fe<sup>III</sup>Cl catalyst on reaction with NO is essential to any meaningful interpretation of the dynamics of the reactions. The ability of (TPP)Fe<sup>III</sup>Cl to remain intact under the reaction conditions was investigated. The reaction of (TPP)Fe<sup>III</sup>Cl (8.2 × 10<sup>-5</sup> M) and NO (27-fold excess over catalyst) was monitored spectrophotometrically at 320 nm, and at its completion, ~30 equiv additional NO was introduced and the reaction again allowed to go to completion. This procedure was repeated until ~120 turnovers had occurred. Figure 7 shows the kinetic results. The calculated value of k<sub>ψ2</sub> is equivalent for all four additions of NO (3.8 × 10<sup>-4</sup> s<sup>-1</sup>) showing that the iron(III)

porphyrin does not lose activity, since it has been shown that the value of k<sub>ψ2</sub> is dependent upon [(TPP)Fe<sup>III</sup>Cl]. Examination of Figure 7 shows that the ΔA<sub>320</sub> for the third and fourth sets of ~30 turnovers (0.21 and 0.07, respectively) are much smaller than the ΔA<sub>320</sub> for the first and second sets of ~30 turnovers (~0.60). Product analysis at completion of each reaction for each NO addition establishes that the observed changes in A<sub>320</sub> which accompany each ~30 turnovers of catalyst are accountable for the percent yields of products. Thus, the changes in ΔA<sub>320</sub> observed after 30, 60, 90, and 120 turnovers were 0.83, 1.43, 1.64, and 1.71, respectively, while the ΔA<sub>320</sub> calculated from the product yields after 30, 60, 90, and 120 turnovers are 0.77, 1.45, 1.85, and 2.06, respectively. Inspection of Table V shows that at above ~100 turnovers of catalyst, there is a falling off of the percent yield of DA, while yields of other products do not change appreciably. Also, there is a loss of material balance at high turnover of *N*-oxide. At 90 turnovers, 12% of the *N*-oxide is unaccounted for, while at 120 turnovers material balance is off by 22%. Clearly, at the highest turnovers, DA is being oxidized to a product which we have failed to identify.

**Time Course for the Formation of Each Product in the (TPP)Fe<sup>III</sup>Cl (7.9 × 10<sup>-5</sup> M) Catalyzed Decomposition of NO (4.3 × 10<sup>-3</sup> M).** Reactions were carried out under argon or nitrogen, and aliquots were withdrawn under flowing argon or nitrogen and stored in dry ice-chilled gas-tight nitrogen-filled vials (see Experimental Section). Plots of concentration vs. time for products DA, MA, FA, H, and MD (determined by HPLC analysis) are shown in Figure 8A–C,E, and F, and a plot of the concentration of CH<sub>2</sub>O vs. time (determined by the Nash assay) is provided in Figure 8D. The correlation lines for the appearance of DA, MA, FA, MD, and CH<sub>2</sub>O represent best fits to the first-order rate law. The correlation line for the formation of H is simply sketched to show the lag in product formation. The first-order rate constants for DA, MA, FA, MD, and CH<sub>2</sub>O formation are compared to the spectrally determined k<sub>ψ2</sub> obtained with the same reaction solution from the change in A<sub>320</sub> with time (see Table VI). The first-order increase in A<sub>320</sub> reflects the fact that over 90% of the change in A<sub>320</sub> is due to the formation of DA, MA, and MD and that the formation of these compounds follows the first-order rate law. The spectrally determined rate constant is equal to the sum of the rate constants times the percentage yield for the formation of the two major products, DA (54%) and MA (25%).

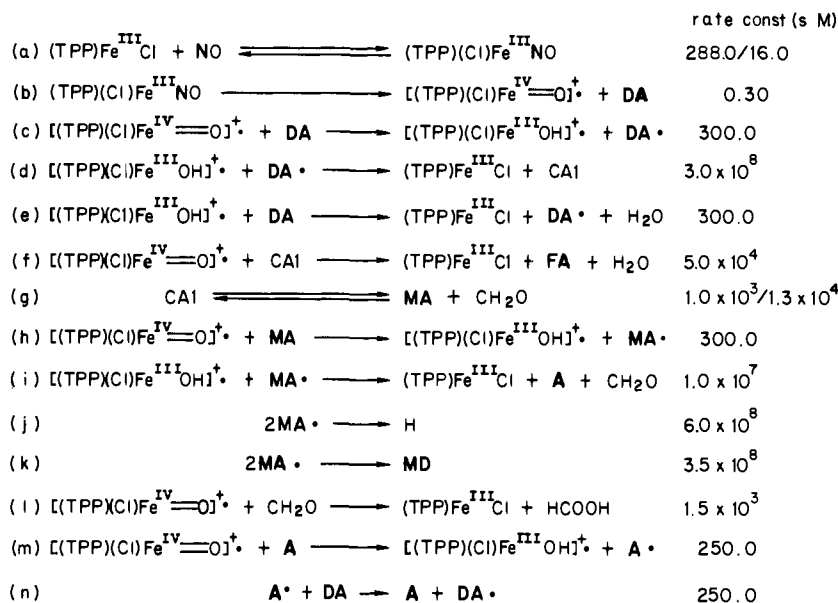
Examination of Figure 8E shows a lag phase in the formation of H and that following the lag phase, there is an accelerated buildup of H. A similar time course was seen for the formation of A and is characteristic of autocatalytic reactions or products formed as the result of sequential reactions. However, in the case of A, it could be simply an artifact due to its proximity to H in the HPLC elution pattern.

The rate constant for the transfer of the "oxene" equivalent from NO to the iron(III) moiety of (TPP)Fe<sup>III</sup>Cl was determined by trapping the [(TPP)(Cl)Fe<sup>IV</sup>=O]<sup>+</sup> species with 2,4,6-tri-*tert*-butylphenol (TBPH) (eq 11). The reaction was monitored by following the formation of TBP• at 630 nm (ε = 400 M<sup>-1</sup> cm<sup>-1</sup> in CH<sub>2</sub>Cl<sub>2</sub>). In separate experiments, it was shown that TBPH does not react with (TPP)Fe<sup>III</sup>Cl nor NO under the conditions of the experiments. The increase in A<sub>630</sub> was found, in all experiments, to follow the first-order rate law to at least 7 × t<sub>1/2</sub>. Inspection of Table VII shows that the apparent first-order rate constant for the appearance of TBP• is independent of [TBPH]<sub>0</sub>, establishing that TBP• is formed after the rate-determining step—a

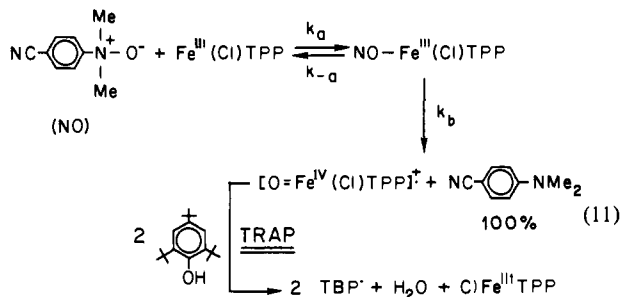


**Table X.** Effect of 2,3-Dimethyl-2-butene (TME) on the Kinetics and Product Yields in the (TPP)Fe<sup>III</sup>Cl (Initial Concentration = 7.6 × 10<sup>-5</sup> M) Catalyzed Decomposition of NO (Initial Concentration = 2.6 × 10<sup>-3</sup> M)

[TME] <sub>0</sub> , M	% yields							<i>k</i> <sub>ψ2</sub> , s <sup>-1</sup>
	DA	MA	H	FA	A	MD	TME oxide	
	57	23	11	2	1	8	0	4.4 × 10 <sup>-4</sup>
0.01	74	17	7	2	1	6	35	4.9 × 10 <sup>-4</sup>
0.1	91	9	2	trace	trace	2	70	5.6 × 10 <sup>-4</sup>
1.0	96	0	0	0	0	0	100	3.3 × 10 <sup>-4</sup>

**Scheme I**

requirement for a trapping experiment. The value of the apparent first-order rate constant (4 ± 2) × 10<sup>-4</sup> s<sup>-1</sup> when divided by

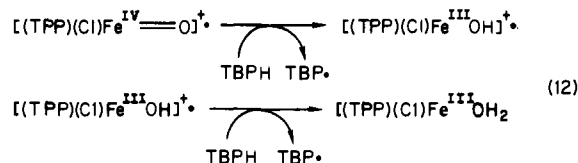


[(TPP)Fe<sup>III</sup>Cl]<sub>0</sub> provides (7 ± 2) M<sup>-1</sup> s<sup>-1</sup> as *k*<sub>a</sub>*k*<sub>b</sub>/*k*<sub>-a</sub> for the bimolecular oxygen atom transfer from *N*-oxide to (TPP)Fe<sup>III</sup>Cl (eq 11). This value may be compared to *k*<sub>ψ2</sub>/[(TPP)Fe<sup>III</sup>Cl] = (5 ± 2) M<sup>-1</sup> s<sup>-1</sup> determined from the increase in *A*<sub>320</sub> with time for all experiments reported in this manuscript and that (7.0 M<sup>-1</sup> s<sup>-1</sup>) calculated from the first-order rate of appearance of DA when divided by [(TPP)Fe<sup>III</sup>Cl].

These comparisons show that oxygen transfer is rate-limiting in the formation of DA. That the second-order rate constant (*k*<sub>ψ2</sub>/[(TPP)Fe<sup>III</sup>Cl]) for *A*<sub>320</sub> vs. time is somewhat smaller than *k*<sub>a</sub>*k*<sub>b</sub>/*k*<sub>-a</sub> (eq 11) is attributed to the fact that the former is based upon the appearance of all absorbing products at 320 nm. Seventy-five percent of Δ*A*<sub>320</sub> is due to the formation of DA, and 25% is due to the appearance of other products which are formed from DA in slower reactions (see Table VI).

The stoichiometry for the trapping experiment was found to be 2 mol of phenoxyl radical produced for each mole of NO used. Therefore, each [(TPP)(Cl)Fe<sup>IV</sup>=O]<sup>+</sup> species is capable of oxidizing two TBPB molecules (eq 12). The mechanism must involve two 1e<sup>-</sup> transfer steps. Thus, the theoretical absorbance at infinite time for the reactions listed in Table VII involving TBPB is 2.08 assuming the 2:1 ratio of TBPB/NO (using a 1-cm cell). For the five runs in Table VII, the final OD was 2.04, 2.09,

2.06, 2.03, and 1.87, respectively. From HPLC analysis, DA is formed in 100% yield as required by eq 11.



That oxygen transfer from NO to (TPP)Fe<sup>III</sup>Cl precedes oxidation of DA has also been determined by the use of deuterium kinetic isotope effects. In these experiments, an intermolecular deuterium kinetic isotope effect was assessed by comparison of the initial rate constants for the reactions of *p*-NCC<sub>6</sub>H<sub>4</sub>N<sup>+</sup>(CH<sub>3</sub>)<sub>2</sub>O<sup>-</sup> and *p*-NCC<sub>6</sub>H<sub>4</sub>N<sup>+</sup>(CD<sub>3</sub>)<sub>2</sub>O<sup>-</sup>, monitored spectrophotometrically at 290 nm with *N*-oxide concentration ranging from 8.6 × 10<sup>-2</sup> to 1.7 × 10<sup>-1</sup> M and the [(TPP)Fe<sup>III</sup>Cl]<sub>0</sub> = 2.7 × 10<sup>-5</sup> M. From the experiments, a calculated second-order rate constant based on initial *N*-oxide concentration of (4.4 ± 0.2) × 10<sup>-3</sup> M<sup>-1</sup> min<sup>-1</sup> was obtained with *p*-NCC<sub>6</sub>H<sub>4</sub>N<sup>+</sup>(CD<sub>3</sub>)<sub>2</sub>O<sup>-</sup> as compared to the rate constant for *p*-NCC<sub>6</sub>H<sub>4</sub>N<sup>+</sup>(CH<sub>3</sub>)<sub>2</sub>O<sup>-</sup> of (4.4 ± 0.2) × 10<sup>-3</sup> M<sup>-1</sup> min<sup>-1</sup>. These results provide an intermolecular isotope effect of ~1.0, establishing that C-H bond breaking is not involved in the rate-determining step.

An intramolecular deuterium kinetic isotope effect was determined by using (TPP)Fe<sup>III</sup>Cl at 1.4 × 10<sup>-4</sup> M and *p*-NCC<sub>6</sub>H<sub>4</sub>N<sup>+</sup>(CH<sub>3</sub>)(CD<sub>3</sub>)O<sup>-</sup> at 4.8 × 10<sup>-3</sup> M and monitoring the formation of *p*-NCC<sub>6</sub>H<sub>4</sub>NH(CD<sub>3</sub>)/*p*-NCC<sub>6</sub>H<sub>4</sub>NH(CH<sub>3</sub>) by GCMS. The value of this ratio was determined at 4.5. An intramolecular deuterium kinetic isotope effect of 4.5 establishes that the demethylation reaction which follows the rate-determining oxygen-transfer step involves considerable C-H bond cleavage.

The ability of NO (2.3 × 10<sup>-3</sup> M) to oxidize the products of its decomposition in the presence of (TPP)Fe<sup>III</sup>Cl (7.6 × 10<sup>-5</sup> M) was investigated. The substrates employed were DA, MA, A, FA, and H (each at 1.0 × 10<sup>-3</sup> M). No appreciable change in the rate constant for an increase in *A*<sub>320</sub> was found on addition of all but

**Table XI.** Comparison of Experimentally Obtained First-Order Rate Constants and Product Yields and the First-Order Rate Constants and Product Yields Obtained by Computer Simulation of Scheme I

	$k_{\psi_2}$ ( $s^{-1}$ )		% Yields	
	Expt.	Calc.	Expt.	Calc.
RNMe <sub>2</sub>	$5.5 \times 10^{-4}$	$3.7 \times 10^{-4}$	54	52
RN(H)Me	$4.0 \times 10^{-4}$	$3.6 \times 10^{-4}$	25	26
CH <sub>2</sub> O	$2.2 \times 10^{-4}$	$3.7 \times 10^{-4}$	12	11
RN-CH <sub>2</sub> -N-R              CH <sub>3</sub> H	$2.8 \times 10^{-4}$	$3.2 \times 10^{-4}$	7	6
RN(Me)-CHO	$2.5 \times 10^{-4}$	$2.9 \times 10^{-4}$	5	5
R-N-N-R          CH <sub>3</sub> CH <sub>3</sub>	- <sup>a</sup>		11	10
RNH <sub>2</sub>	- <sup>b</sup>		4	7
$\Delta A_{320}$	$4.4 \times 10^{-4}$	$3.9 \times 10^{-4}$		

[NO] =  $4.3 \times 10^{-3}$  M      [TPPF<sup>III</sup>Cl] =  $7.9 \times 10^{-5}$  M

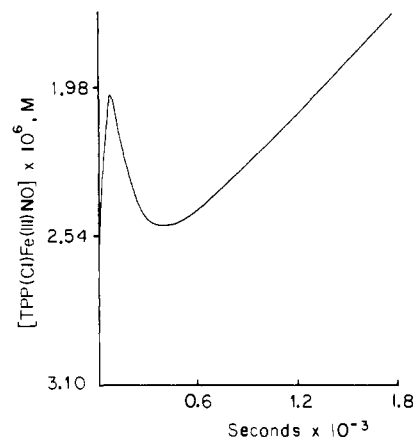
<sup>a</sup>Sigmoidal time course seen experimentally is predicted by simulation. <sup>b</sup>Sigmoidal time course is not predicted by simulation and may be an experimental artifact due to the closeness of the elution times of H and A.

A. The addition of A to the reaction mixture, at a concentration equal to that formed from NO in turnover experiments, had no effect on  $k_{\psi_2}$ . However, at a concentration of A which greatly exceeds that formed in the decomposition experiments with the *N*-oxide, there was inhibition so that  $k_{\psi_2}$  was approximately one-third of that seen in its absence (Table VIII).

The percent yields of products formed on decomposition of NO are not influenced by the addition of FA, H, or DA (Table VIII), whereas the addition of MA and A drastically changes the product composition. The computation of the percent yields of Table VIII was carried out in the following manner: For DA, FA, H, and A, the yields were calculated after subtraction of the added reagent and are based upon [NO]<sub>i</sub>. Addition of DA, FA, and H does not change the product composition. When MA is added, the percentage yields of products, based upon [NO]<sub>i</sub>, add up to more than 100%. This is so because MA is being consumed. The oxidation of added MA is seen to result in a 3- to 4-fold increase in the yield of H and MD. Inspection of Table VIII shows that the addition of A blocks the oxidation of the MA formed by decomposition of NO. This results in a greater yield of MA and no detectable yield of its oxidation products H, FA, and A. This effect of A on the products of decomposition of NO is not seen at the concentrations of NO employed in the turnover experiments in our study.

In separate experiments, the ability of the various products of *N*-oxide decomposition to complex (TPP)Fe<sup>III</sup>Cl was studied at 410 nm. An excess of the decomposition product (in comparison to the amount that is formed during 30 turnovers of catalyst) was added to the (TPP)Fe<sup>III</sup>Cl ( $7.9 \times 10^{-5}$  M). In no case was an effect on the Soret band of (TPP)Fe<sup>III</sup>Cl at 410 nm seen, allowing one to conclude that no measurable complexation to the iron(III) porphyrin occurred.

The oxidation of a variety of alkenes and cyclohexane by NO ( $2.0 \times 10^{-2}$  M) and (TPP)Fe<sup>III</sup>Cl ( $2.0 \times 10^{-3}$  M) in grade A CH<sub>2</sub>Cl<sub>2</sub> at 25 °C under a N<sub>2</sub> atmosphere was determined by capillary GC (see Experimental Section). The products were obtained in comparable yields to those previously reported with iodobenzene<sup>2a,28</sup> (Table IX). The stereospecificity seen with iodobenzene is also evidenced with NO.<sup>3</sup> As would be anticipated, the yield of dealkylation product (determined by capillary GC) decreases in the presence of alkene. In the presence of 0.8



**Figure 9.** Time course of the (TPP)(Cl)Fe<sup>III</sup>NO complex produced by computer simulation of Scheme I where [(TPP)Fe<sup>III</sup>Cl]<sub>i</sub> =  $7.5 \times 10^{-5}$  M and [NO]<sub>i</sub> =  $2.5 \times 10^{-3}$  M.

M 2,3-dimethyl-2-butene, essentially no dealkylation was observed and 2,2,3,3-tetramethyloxirane and DA were obtained in 90% and 100% yields, respectively.

The reaction of 2,3-dimethyl-2-butene (TME) with NO in the presence of (TPP)Fe<sup>III</sup>Cl was chosen for an in-depth study. The addition of TME as a substrate in the (TPP)Fe<sup>III</sup>Cl-catalyzed decomposition of NO has no effect on the kinetics of this reaction; i.e.,  $k_{\psi_2}$  from the change in  $A_{320}$  with time is the same in the absence ( $4.4 \times 10^{-4}$  s<sup>-1</sup>) or presence ( $4.6 \times 10^{-4}$  s<sup>-1</sup>) of TME at an [(TPP)Fe<sup>III</sup>Cl]<sub>i</sub> =  $7.6 \times 10^{-5}$  M. However, the product ratios are, as is to be expected, dependent on the [TME]<sub>i</sub> (see Table X). The higher the [TME]<sub>i</sub>, the higher the yield of epoxide (TME oxide) and DA. In fact, at 1.0 M TME the only products formed are DA and TME oxide (from GC and HPLC analysis). As the initial concentration of TME is lowered, the lower the yield of DA and TME oxide becomes. Other oxidation products are obtained in their stead (see Table X).

**Discussion and Kinetic Simulation.** In the presence of (tetraphenylporphyrinato)iron(III) chloride [(TPP)Fe<sup>III</sup>Cl] in dichloromethane solvent at 25 °C, *p*-cyano-*N,N*-dimethylaniline *N*-oxide (NO) decomposes to *p*-cyano-*N,N*-dimethylaniline (DA), *p*-cyano-*N*-methylaniline (MA), *p*-cyano-*N*-formyl-*N*-methylaniline (FA), *p*-cyanoaniline (A), *N,N'*-bis(*p*-cyanophenyl)-*N*-methylmethylenediamine (MD), *N,N'*-dimethyl-*N,N'*-bis(*p*-cyanophenyl)hydrazine (H), and formaldehyde. At [NO] =  $2.6 \times 10^{-3}$  to  $5.1 \times 10^{-3}$  M and [(TPP)Fe<sup>III</sup>Cl] =  $7.0 \times 10^{-5}$  M, the percentage yields of the various products of NO decomposition are not influenced by the presence of O<sub>2</sub>. The experimental results (Table III) are summarized:

	% yields of prod based upon [NO] <sub>i</sub>					
	DA	MA	H	A	FA	MD
anaerobic	56	31	12	2	4	6
aerobic	55	29	12	2	4	6

It should be pointed out that the total yields exceed 100% due to the experimental error that exists in the HPLC analysis technique. Under the given concentrations of reactants, the dynamics of the decomposition of the *N*-oxide are also insensitive to the presence or absence of O<sub>2</sub> (Table III). Nevertheless, all measurements have been carried out under N<sub>2</sub> or argon atmosphere. The importance of solvent purity has also been examined (Experimental Section). The rate of (TPP)Fe<sup>III</sup>Cl catalysis of *N*-oxide decomposition is also (surprisingly) insensitive to solvent purity (Table II). In this study, four grades of solvent were employed: (i) technical grade (D); (ii) Aldrich Gold Label (C); (iii) an extensively purified solvent (B); and (iv) the same extensively purified solvent passed through a dry alumina column just prior to use (A). In the C and, particularly, D solvents, the number of detectable products were increased due, undoubtedly, to oxidative conjugation of intermediates with solvent impurities, as shown by a decreased yield of MA (Table I).

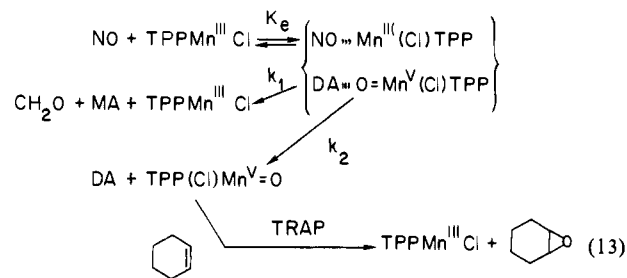
The decomposition of NO in the presence of (TPP)Fe<sup>III</sup>Cl may be followed by HPLC analysis of products with time and, conveniently, by monitoring the increase of absorbance at 320 nm with time. The successful use of the latter procedure is dependent upon the lack of appreciable absorbance of (TPP)Fe<sup>III</sup>Cl at 320 nm and the finding that the products of NO decomposition absorb appreciably at 320 nm. The change in absorbance at 320 nm during the course of reaction has been shown to be quantitatively accountable by the concentration of the products formed with time (Table III). From the increase in  $A_{320}$  with time, the reaction has been shown to be first order in both NO and (TPP)Fe<sup>III</sup>Cl, showing that the (TPP)Fe<sup>III</sup>Cl catalyst does not become saturated with NO (Figure 5). No decrease in iron(III) porphyrin catalytic efficiency was seen for reactions involving up to 120 turnovers of NO (Figure 7).

That the rate-determining step involves oxygen transfer from NO to (TPP)Fe<sup>III</sup>Cl is shown by the data collected from three types of experiments. First, employing 2,4,6-tri-*tert*-butylphenol to trap the intermediate [(TPP)(Cl)Fe<sup>IV</sup>=O]<sup>+</sup> species (eq 11) formed during continual turnover of catalyst gave a second-order rate constant ( $k_{\text{obsd}}/[(\text{TPP})\text{Fe}^{\text{III}}\text{Cl}]_i$ ) of  $7 (\pm 2) \text{ M}^{-1} \text{ s}^{-1}$ . This constant is identical with the second-order rate constant of  $7.0 \text{ M}^{-1} \text{ s}^{-1}$  for the formation of DA with time during continual turnover of catalyst. Second, the rate of epoxidation of 2,3-dimethyl-2-butene (TME) is independent of its concentration (0.01–1.0 M). Similar results were obtained for the oxidation of MA by NO in the presence of (TPP)Fe<sup>III</sup>Cl catalyst. Third, the use of deuterium kinetic isotope effects also supports oxygen transfer from NO to (TPP)Fe<sup>III</sup>Cl as rate limiting. Comparison of initial rate constants for the reactions of *p*-NCC<sub>6</sub>H<sub>4</sub>N<sup>+</sup>(CH<sub>3</sub>)<sub>2</sub>O<sup>-</sup>/*p*-NCC<sub>6</sub>H<sub>4</sub>N<sup>+</sup>(CD<sub>3</sub>)<sub>2</sub>O<sup>-</sup> with (TPP)Fe<sup>III</sup>Cl yielded an intermolecular isotope effect of  $\sim 1.0$ , establishing that no C–H bond breaking (demethylation of DA) is involved in the rate-determining step for the decomposition of NO.

The formation of DA, MA, FA, MD, and CH<sub>2</sub>O each follows the first-order rate law. The pseudo-first-order rate constants for the formation of each product lie quite close to the first-order rate constant determined from the change in absorbance of the reaction mixture at 320 nm with time (Table VI). The latter constant is determined principally by the appearance of the major products DA and MA. The appearance of H is associated with a lag phase followed by a continual acceleration of its formation with depletion of starting *N*-oxide. Sigmoidal appearance of a product with time suggests either autocatalysis or that the product arises from a sequence of reactions whose rates are rate-determining for the product formation.

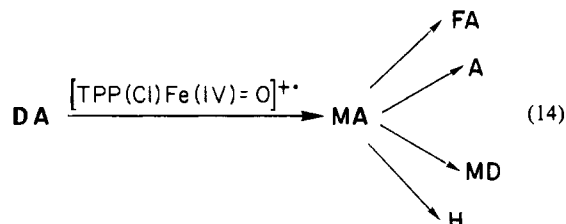
Presumably, ligation of the *N*-oxide to the (TPP)Fe<sup>III</sup>Cl occurs prior to oxygen transfer. To obtain information concerning the magnitude of the equilibrium constant for complexation of the *N*-oxide to (TPP)Fe<sup>III</sup>Cl, we have employed picoline *N*-oxide (PNO). The equilibrium constants  $K_1$  and  $\beta_2$  corresponding to the complexation of one and two PNO moieties were found to be 18 and  $79 \text{ M}^{-1}$ , respectively (see eq 8 and 9, Results section). At PNO concentrations equal to the NO concentrations used in the present study, the mono-*N*-oxide complex would exceed the di-*N*-oxide complex by  $\sim 100$ . It is not unreasonable to assume, therefore, that oxygen transfer from NO to (TPP)Fe<sup>III</sup>Cl occurs within a 1:1 complex of these species (eq 11).

The reaction of NO with (TPP)Fe<sup>III</sup>Cl (CH<sub>2</sub>Cl<sub>2</sub> solvent) differs from the reaction of NO with (TPP)Mn<sup>III</sup>Cl (benzonitrile solvent). When (TPP)Mn<sup>III</sup>Cl reacts with NO in the presence of cyclohexene, it is found that any DA oxidation occurs prior to formation of free [(TPP)(Cl)Mn<sup>V</sup>=O] which is trapped by the alkene (eq 13).<sup>1</sup> In the [(TPP)(Cl)Fe<sup>IV</sup>=O]<sup>+</sup> trapping experiments with 2,4,6-tri-*tert*-butylphenol (TBPH), DA is produced in 100% yield to the exclusion of the products (MA, FA, A, MD, and H) seen in the absence of TBPH. With 1.0 M TME, there was obtained in 100% yields the TME epoxide and DA. Thus, experimental evidence suggests that aside from DA, the additional products of NO decomposition are derived from the direct oxidation of DA and do not arise upon decomposition of the complex of NO and iron(III) porphyrin. If decomposition products arose from the

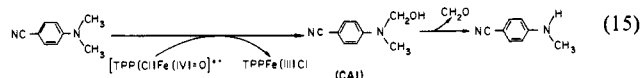


NO iron(III) porphyrin complex directly (as seen in the reaction of NO with (TPP)Mn<sup>III</sup>Cl in eq 13), then the yield of DA would be determined by the ratio of  $k_1/k_2$ , and the addition of a [(TPP)(Cl)Fe<sup>IV</sup>=O]<sup>+</sup> trap such as TBPH or TME would not result in an increase in DA (to 100% as observed). Therefore, the "cascade" of products arises from DA oxidation by [(TPP)(Cl)Fe<sup>IV</sup>=O]<sup>+</sup>.

A better understanding of the "cascade" of oxidations commencing with the oxidation of DA was obtained from the investigation of the ability of the [(TPP)(Cl)Fe<sup>IV</sup>=O]<sup>+</sup> species to oxidize the products of NO decomposition. The only product to be oxidized was MA, suggesting that all the other products—FA, A, MD, and H—came about from the further "oxidation" of MA and are end products. Thus, the reaction scheme can be elaborated upon (eq 14).



Analysis of the NO/(TPP)Fe<sup>III</sup>Cl reaction mixture revealed the first-order formation of CH<sub>2</sub>O during the decomposition of the *N*-oxide. Thus, the demethylation of DA and MA involves carbinolamine intermediates which upon loss of CH<sub>2</sub>O yield MA and A, respectively (as in eq 15 for DA). The C–H bond breaking



in the demethylation of DA is associated with a discriminatory (intramolecular) deuterium kinetic isotope effect. Thus, when the reaction was performed by using *p*-NCC<sub>6</sub>H<sub>4</sub>N<sup>+</sup>(CH<sub>3</sub>)(CD<sub>3</sub>)O<sup>-</sup>, the ratio of MA products (*p*-NCC<sub>6</sub>H<sub>4</sub>NH(CH<sub>3</sub>)/(*p*-NCC<sub>6</sub>H<sub>4</sub>NH(CD<sub>3</sub>)) =  $k^{\text{H}}/k^{\text{D}}$  was 4.5. Intramolecular discriminatory isotope effects accompanying demethylation on reaction of *p*-NCC<sub>6</sub>H<sub>4</sub>N<sup>+</sup>(CH<sub>3</sub>)(CD<sub>3</sub>)O<sup>-</sup> and C<sub>6</sub>H<sub>4</sub>N<sup>+</sup>(CH<sub>3</sub>)(CD<sub>3</sub>)O<sup>-</sup> with cytochromes P-450<sub>LM2</sub> and P-450<sub>CAM</sub> have been found to range from 2.0 to 4.3.<sup>17</sup> On reaction of cytochrome P-450<sub>LM2</sub> (NADPH + O<sub>2</sub>) with *p*-NCC<sub>6</sub>H<sub>4</sub>N(CH<sub>3</sub>)(CD<sub>3</sub>) and C<sub>6</sub>H<sub>4</sub>N(CH<sub>3</sub>)(CD<sub>3</sub>), the discriminatory isotope effects were determined to be 3.9 and 2.6, respectively.

Intramolecular isotope effects have been reported by Miwa et al.<sup>29</sup> for the cytochrome P-450 and peroxidase-catalyzed *N*-demethylation of *N*-methyl-*N*-(trideuteriomethyl)aniline. The isotope effects for the peroxidases (H<sub>2</sub>O<sub>2</sub>, EtO<sub>2</sub>H), hemoglobin (EtO<sub>2</sub>H), and myoglobin (EtO<sub>2</sub>H) were large ( $k_{\text{H}}/k_{\text{D}} > 8.5$ ), while those for the cytochrome P-450 (NADPH + O<sub>2</sub>, cumyl hydroperoxide) were low ( $k_{\text{H}}/k_{\text{D}} < 3.1$ ). The kinetic isotope effects for direct H• abstraction (permanganate with  $\alpha$ -dideuterio-benzylamine,<sup>30</sup> cytochrome P-450 aliphatic hydroxylation,<sup>31,32</sup> and O-demethylation<sup>33,34</sup>) range between 7.0 and 11.5, while oxidations

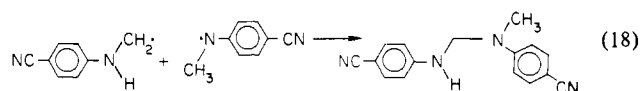
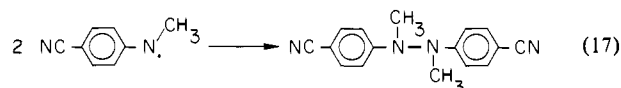
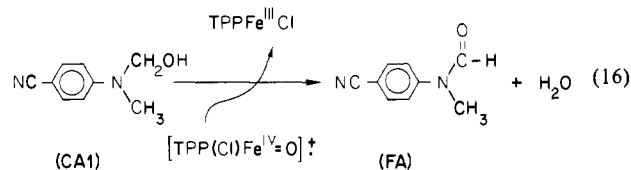
(29) Miwa, G. T.; Walsh, J. S.; Kedderis, G. L.; Hollenberg, P. F. *J. Biol. Chem.* **1983**, *258*, 14445.

(30) Wei, M. M.; Stewart, R. *J. Am. Chem. Soc.* **1966**, *88*, 1974.

(31) Groves, J. T.; McCluskey, G. A.; White, R. E.; Coon, M. J. *Biochem. Biophys. Res. Commun.* **1978**, *81*, 154.

involving anilinium radical formation followed by deprotonation range between 1.3 and 3.6 (chlorine dioxide with benzylamines,<sup>35</sup> permanganate with trimethylamine,<sup>36</sup> and oxidation of *N*-methyl-di-*N*-butylamine by alkaline potassium ferricyanide<sup>37</sup>). By analogy, the discriminatory kinetic isotope effect of 4.4 observed in this study would appear to represent one-electron oxidation of DA followed by deprotonation. It should be pointed out that the discriminatory isotope effect for DA oxidation does not indicate whether electron transfer or deprotonation is rate-determining.

Formation of FA results from further oxidation of the intermediate carbinolamine in DA oxidation (eq 16), while MD and H most likely result from the radical coupling of two MA<sup>•</sup> moieties (eq 17 and 18).



**Kinetic Simulation.** By the coupling of the individual reactions, there is obtained, by digital computer simulation (see Experimental section) the thermodynamic (eq a and g) and kinetic constants (eq b-f, h-n) of Scheme I. Computations with Scheme I mimic the various experimental observations for the reactions of NO with (TPP)Fe<sup>III</sup>Cl.

(1) A computer plot, generated from Scheme I, of the combined concentrations of *p*-cyano-*N,N*-dimethylaniline (DA), *N*-formyl-*p*-cyano-*N*-methylaniline (FA), *p*-cyano-*N*-methylaniline (MA), *N,N'*-dimethyl-*N,N'*-bis(*p*-cyanophenyl)hydrazine (H), *N,N'*-bis(*p*-cyanophenyl)-*N*-methylmethylenediamine (MD), and *p*-cyanoaniline (A) (each multiplied by their respective extinction coefficients at 320 nm) is superimposable on a plot of  $A_{320}$  vs. time for given concentrations of NO and (TPP)Fe<sup>III</sup>Cl obtained experimentally. Thus, the equation and rate constants in Scheme I predict correctly the experimentally obtained  $k_{\psi 2}$  (Table XI). Further, changing [NO] is predicted to change  $\Delta A_{320}$  but not  $k_{\psi 2}$  nor the percentage yields of products. The decrease in the percent yield of DA at over >100 turnovers, seen experimentally, is not predicted, nor should it be, since there has not been included a step for the conversion of a small portion of DA to a product which we have yet to identify (see Results section).

(2) Increasing the [(TPP)Fe<sup>III</sup>Cl]<sub>i</sub> (from  $3.1 \times 10^{-5}$  to  $5.0 \times 10^{-4}$  M) at a constant [NO]<sub>i</sub> ( $3.0 \times 10^{-3}$  M) increases  $k_{\psi 2}$  in a linear fashion. The slopes of plots when using experimental and simulated rate data are identical.

(3) The predicted formations of DA, MA, FA, and CH<sub>2</sub>O are first-order and the rate constants obtained by fitting the computer-drawn plots of concentration vs. time for appearance of each product to the first-order rate law are in agreement with the rate constants determined by HPLC (Table XI). Furthermore, this agreement is within the accuracy of the HPLC analysis (a factor of 1.0–1.7). In the case of the formation of H, a lag phase is

predicted as seen experimentally.

(4) Simulation of the appearance of [(TPP)(Cl)Fe<sup>III</sup>NO] vs. time using Scheme I provides some rationale for the time-dependence change in the Soret band at  $A_{410}$  experimentally observed on mixing NO with (TPP)Fe<sup>III</sup>Cl. This can be seen by comparison of Figures 2 and 9. Examination of these figures shows that the initial and very rapid drop in  $A_{410}$  followed by its exponential increase, then decrease, and subsequent increase can be tentatively ascribed to the appearance, disappearance, reappearance, and subsequent disappearance of (TPP)(Cl)Fe<sup>III</sup>NO. The divergence of the plots in Figures 2 and 9 can be accounted for by a slow ligand exchange of Cl<sup>-</sup> for H<sub>2</sub>O that is produced in the oxidation of DA to products. The final porphyrin spectrum at the completion of the reaction shows that some (TPP)Fe<sup>III</sup>Cl has been converted to [(TPP)Fe<sup>III</sup>]<sub>2</sub>O. In a following paper, we show that aside from a small lag phase, the turnover of NO by [(TPP)Fe<sup>III</sup>]<sub>2</sub>O has the same rate constant as seen when using (TPP)Fe<sup>III</sup>Cl. For this reason, the small amount of ligand exchange that occurs has not and needs not be considered.

(5) To account for the experimental observation that addition of A to the reaction mixture (at  $t_0$ ) in concentration ( $1 \times 10^{-3}$  M) greatly exceeding its percent yield, prevents the oxidation of MA, it is required that a [(TPP)(Cl)Fe<sup>IV</sup>=O]<sup>•</sup> is converted by A to an oxidant that oxidized DA → MA but does not effectively oxidize MA. Such a requirement is found in the oxidation of A to its cation radical followed by oxidation of DA by both A<sup>•</sup> and [(TPP)(Cl)Fe<sup>III</sup>=O]<sup>•</sup>. The reactions of eq m and n in Scheme I accommodate this need and account quantitatively for the experimental observations.

Restrictions on the numerical values of the rate constants of Scheme I may now be considered as can the reasonableness of the individual reactions and the magnitude of the various constants. The value of  $k_a k_b / k_{-a}$  (the respective rate constants for reactions a and b) determines the rate of NO disappearance, since it has been shown that reaction b is rate-determining. It can be shown, by computer simulation, that for preequilibrium formation of (TPP)(Cl)Fe<sup>III</sup>NO to precede rate-determining intracomplex oxygen transfer,  $k_b / k_{-a}$  cannot exceed  $1/10$  and  $k_{-a}$  cannot exceed  $k_a$ . The value of  $18 \text{ M}^{-1}$  chosen for  $k_a / k_{-a}$  is the experimentally determined equilibrium constant for complexation of picoline *N*-oxide with (TPP)Fe<sup>III</sup>Cl (Results section). This requires  $k_b$  to equal  $0.3 \text{ s}^{-1}$  so that  $k_b / k_{-a} \cong 1/50$ . The absolute values of  $k_a$  and  $k_{-a}$  used meet the kinetic requirements and, importantly, allow approximate simulation (Figure 9) of the oscillatory concentration of iron(III) porphyrin *N*-oxide complex seen experimentally (Figure 2).

The ratios of the rate constants given for reactions c–l (Scheme I) provide the correct percent yields of the products DA, MA, MD, FA, H, and A (see Table XI). The absolute values of the constants, keeping their ratios appropriately constant, can be varied by less than 2-fold. The unfavorable equilibrium constant for dissociation of CA1 to MA and CH<sub>2</sub>O in eq g is absolutely required in order that Scheme I provide the experimentally observed rate constant for FA appearance. However, the absolute value for  $k_g$  and  $k_{-g}$  is not important; i.e.,  $k_g / k_{-g}$  must be  $1/13$  but the rate constants can range in magnitude from  $10.0/130.0$  to  $1 \times 10^8/1.3 \times 10^9$  without affecting the overall computations within Scheme I. The constants  $k_m$  and  $k_n$  are those required to account for the change in product ratios on addition of A and, given the constants  $k_c$ – $k_l$ , have no numerical play. Thus, the 14 rate constants of Scheme I possess the required values to reproduce the percent yield and rates of product formation (loc. cit.), and none may be considered terribly soft.

The chemistry of the individual steps in Scheme I may now be considered. Preequilibrium complexation of NO and (TPP)Fe<sup>III</sup>Cl and rate-determining transfer of oxygen from *N*-oxide to iron porphyrin have been amply discussed. Reactions c, d and h, i describe the oxidations of *p*-cyano-*N,N*-dimethylaniline (DA) and *p*-cyano-*N*-methylaniline (MA), respectively. One-electron transfer from DA or MA to the higher valent iron oxoporphyrin  $\pi$ -cation radical is shown to be rate-determining (step c) in dealkylation, since the following oxidation of DA<sup>•</sup> or MA<sup>•</sup> (step d)

(32) Hjelmeland, L. M.; Aronow, L.; Trudell, J. R. *Biochem. Biophys. Res. Commun.* **1977**, *76*, 541.

(33) Foster, A. B.; Jannan, M.; Stevens, J. D.; Thomas, P.; Westwood, J. H. *Chem. Biol. Interact.* **1974**, *9*, 327.

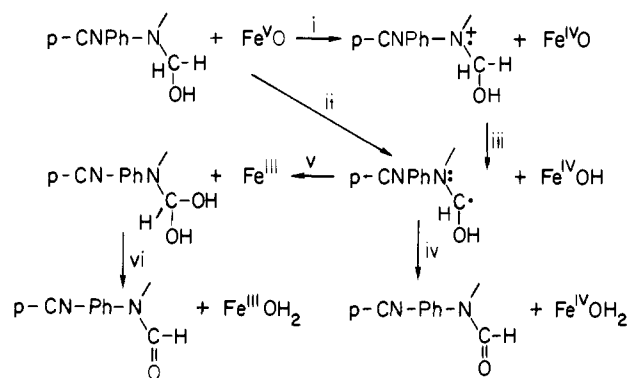
(34) Watanabe, Y.; Oae, S.; Iyanagi, T. *Bull. Chem. Soc. Jpn.* **1982**, *55*, 188.

(35) Hull, L. A.; Davis, G. T.; Rosenblatt, D. H.; Williams, H. K. R.; Weglein, R. C. *J. Am. Chem. Soc.* **1967**, *89*, 1163.

(36) Rosenblatt, D. H.; Davis, G. T.; Hull, L. A.; Forberg, G. D. *J. Org. Chem.* **1968**, *33*, 1649.

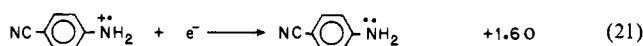
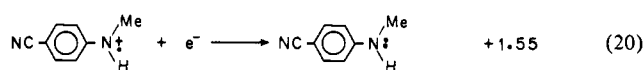
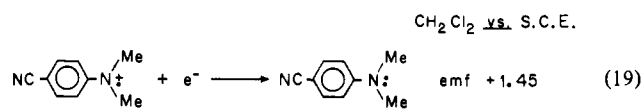
(37) Lindsay Smith, J. R.; Mead, L. A. V. *J. Chem. Soc., Perkin Trans. 2* **1973**, 206.

## Scheme II



exceeds the rate constant for conversion of  $DA \rightarrow DA\cdot$  and  $MA \rightarrow MA\cdot$  by  $10^6$ . Ample evidence exists in the literature for a rate-limiting one-electron transfer in the two-electron oxidation of *N*-alkylamines.<sup>38-40</sup> The rate constant of  $300 \text{ M}^{-1} \text{ s}^{-1}$  for one-electron transfer from  $DA$  and  $MA$  to  $[(\text{TPP})(\text{Cl})\text{Fe}^{\text{IV}}=\text{O}]^+$  is quite reasonable because of the electron-withdrawing *p*-cyano substituent. Thus, compound I of horseradish peroxidase, which possesses at its active site an iron(IV) protoporphyrin(IX)  $\pi$ -cation radical, rapidly oxidizes *N,N*-dimethylaniline but does not oxidize *p*-cyano-*N,N*-dimethylaniline.<sup>41,42</sup> In a model study<sup>15</sup> it has been shown that *N,N*-dimethylaniline *N*-oxide in the presence of  $(\text{TPP})\text{Fe}^{\text{III}}\text{Cl}$  catalyst is unable to epoxidize 2,3-dimethyl-2-butene (TME, 1.0 M) due to the fact that the generated *N,N*-dimethylaniline reacts preferentially with the higher valent iron oxoporphyrin. In this study, however, we show that in the presence of 1.0 M TME, *p*-cyano-*N,N*-dimethylaniline *N*-oxide/ $(\text{TPP})\text{Fe}^{\text{III}}\text{Cl}$  yields 100% epoxide to the exclusion of any oxidation of the generated  $DA$ . These results establish the difficulty in the oxidation of  $DA$ .

Dr. T. Calderwood, in this laboratory,<sup>43</sup> has determined the following potentials for the one-electron oxidation of *p*-cyanoanilines in the solvent ( $\text{CH}_2\text{Cl}_2$ ) employed in the study: The



oxidation potentials of  $DA$ ,  $MA$ , and  $A$  differ by only 50 mV,<sup>43</sup> so that the similarity in the rate constants for the one-electron oxidation reactions c, h, and m is reasonable. He has also shown that the potentials for the reduction of  $[(\text{TPP})(\text{Cl})\text{Fe}^{\text{III}}\text{X}]^+$  and  $[(\text{TPP})(\text{Cl})\text{Fe}^{\text{III}}\text{X}]^{2+}$  are comparable to the reduction potentials for the aniline cation radicals. This supports the contention that the oxidation of  $DA$  and  $MA$  by  $[(\text{TPP})(\text{Cl})\text{Fe}^{\text{IV}}=\text{O}]^+$  should not be greatly favored thermodynamically. The oxidation of  $DA$  by an electrochemically generated  $[(\text{TPP})(\text{Cl})\text{Fe}^{\text{III}}\text{X}]^+$  has been shown to occur.<sup>43</sup>

**Table XII.** Comparison of the Second-Order Rate Constants for the Epoxidation of Alkenes by  $[(\text{TPP})(\text{Cl})\text{Fe}^{\text{IV}}=\text{O}]^+$  and MCPBA in  $\text{CH}_2\text{Cl}_2$

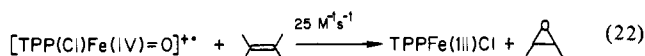
alkene	est rate const with $[(\text{TPP})(\text{Cl})\text{Fe}^{\text{IV}}=\text{O}]^+$ , $\text{M}^{-1} \text{ s}^{-1}$	lit val with MCPBA, $\text{M}^{-1} \text{ s}^{-1}$
	25.0	(10) <sup>a</sup>
	12.5	$2.3 \times 10^{-2b}$
	10.0	$5.4 \times 10^{-2c}$
	8.1	
	4.7	$3.6 \times 10^{-3d}$

<sup>a</sup> In separate experiments, the rate constant (25 °C) for epoxidation of 2,3-dimethyl-2-butene (TME) by *m*-chloroperoxybenzoic acid (MCPBA) was determined in ethanol as  $0.1 \text{ M}^{-1} \text{ s}^{-1}$  and in  $\text{CH}_2\text{Cl}_2$  to exceed  $2.6 \text{ M}^{-1} \text{ s}^{-1}$  (using the iodometric assay employed in the previous study: Bruice, T. C.; Noar, J. B.; Ball, S. S.; Venkataram, U. V. *J. Am. Chem. Soc.* **1983**, *105*, 2452 under the pseudo-first-order conditions of  $[\text{TME}] \gg [\text{MCPBA}]$ . It has previously been shown (see ref 44 of manuscript) that transfer from alcohol to  $\text{CH}_2\text{Cl}_2$  provides approximately 100-fold rate enhancement in the epoxidation of alkenes by *m*-chloroperoxybenzoic acid. Thus, the rate constant in the table has been obtained by multiplying the rate constant obtained in ethanol by 100. <sup>b</sup> Determined at 20 °C in  $\text{CH}_2\text{Cl}_2$  (see ref 45). <sup>c</sup> Determined by the method of competitive rates in  $\text{CH}_2\text{Cl}_2$  at ambient temperature (see ref 46). <sup>d</sup> Determined in  $\text{CH}_2\text{Cl}_2$  at 30 °C (see ref 44).

The formation of *N*-formyl-*p*-cyano-*N*-methylaniline (FA) is shown in reaction f. It would appear that this is the only reasonable means of obtaining FA. Possible steps in the mechanism of this oxidation are shown in Scheme II. Of the four possible mechanisms, the two preceding through one-electron oxidation on nitrogen (i) can probably be eliminated in favor of H $\cdot$  abstraction from carbon (ii).

Thus, comparison of the second-order rate constants for the one-electron oxidation of  $DA$  and  $CAI$  shows the latter to be more rapid by a factor of  $\sim 10^2$ , yet the carbinolamine hydroxyl group through its inductive withdrawal of electrons should actually slow the one-electron oxidation on nitrogen. The presence of the oxygen lone pairs in the carbinolamine radical are not likely to provide a stabilizing effect on a carbon radical since a carbon radical is more stable than an oxygen radical. Of the remaining two possibilities, (ii, iv) vs. (ii, v, vi), the latter represents the rebound mechanism<sup>8,9</sup> proposed by Groves for the hydroxylation of hydrocarbons. The rate constants for the radical coupling reactions j and k are diffusion-controlled as expected.

From the simulation of the kinetics of the reaction of  $\text{NO}$  with  $(\text{TPP})\text{Fe}^{\text{III}}\text{Cl}$ , it has been possible to calculate a second-order rate constant for the oxidation of *p*-cyano-*N,N*-dimethylaniline, *p*-cyano-*N*-methylaniline, and *p*-cyanoaniline by  $[(\text{TPP})(\text{Cl})\text{Fe}^{\text{IV}}=\text{O}]^+$ . The ability to determine quantitatively the second-order rate constants for oxidations by iron(IV) porphyrin cation radicals is required if one wishes to understand the effects of porphyrin structure and ligation upon the reactivity of the higher valent iron oxoporphyrin species. From the experimental data of this study, it is also possible to calculate the second-order rate constants for the reaction of  $[(\text{TPP})(\text{Cl})\text{Fe}^{\text{IV}}=\text{O}]^+$  with the hydrocarbon substrates in Table IX. Thus, addition of eq 22 to Scheme I allows the simulation of the experimental results of Table X within 2% of the experimental percent yields of  $DA$ ,  $MA$ , and  $TME$  oxide. The relative rates (to TME) for the reaction of the



(44) Schwartz, N. N.; Blumbergs, J. N. *J. Org. Chem.* **1964**, *29*, 1976.

(45) Renolen, P.; Ulgestad, J. *J. Chem. Phys.* **1960**, *32*, 634.

(46) Sharpless, K. B.; Townsend, J. M.; Williams, D. R. *J. Am. Chem. Soc.* **1972**, *94*, 295.

(38) Davis, G. T.; Demek, M. M.; Rosenblatt, D. H. *J. Am. Chem. Soc.* **1972**, *94*, 3321.

(39) Audeh, C. A.; Lindsay Smith, J. R. *J. Chem. Soc. B* **1971**, 1741.

(40) Galliani, G.; Rindone, B.; Beltrame, P. L. *J. Chem. Soc., Perkin Trans. 2* **1976**, 1803.

(41) Galliani, G.; Rindone, B.; Marchesini, A. *J. Chem. Soc., Perkin Trans. 1* **1978**, 456.

(42) Galliani, G.; Rindone, B. *Bioorg. Chem.* **1981**, *10*, 283.

(43) Calderwood, T. S.; Bruice, T. C., unpublished results.

other hydrocarbons of Table IX can then be approximated from their percentage yields (Table XII). Included in Table XII for comparison are rate constants for epoxidation of the various alkenes by *m*-chloroperoxybenzoic acid (MCPBA). Inspection of Table XII shows that the [(TPP)(Cl)Fe<sup>IV</sup>=O]<sup>+</sup> species is more reactive and less selective as an epoxidizing agent than is MCPBA. Though there are few rate constants available for comparison, the data that are available provide the linear free energy relationship of eq 23. The reactivity of the [(TPP)(Cl)Fe<sup>IV</sup>=O]<sup>+</sup>.

$$\log k_{[(\text{TPP})(\text{Cl})\text{Fe}^{\text{IV}}=\text{O}]^+} = 0.3 \log k_{\text{MCPBA}} + 1.4 \quad (23)$$

is obviously much less sensitive to the nucleophilicity of the alkene than is *m*-chloroperoxybenzoic acid.

**Acknowledgment.** This work was supported by a grant from the National Institutes of Health.

**Note Added in Proof.** The results of this study establish without doubt that the *N*-oxide of *p*-cyano-*N,N*-dimethylaniline transfers

an oxygen atom to *meso*-(tetraphenylporphinato)iron(III) chloride quantitatively. The arguments by Burka et al.<sup>47</sup> that this is not so must now be considered as erroneous.

**Registry No.** NO, 62820-00-2; DA, 1197-19-9; MA, 4714-62-9; MA ethyl carbamate derivative, 97860-70-3; MA-methyl-*d*<sub>3</sub> ethyl carbamate derivative, 97860-71-4; MA-methyl-*d*<sub>3</sub>, 97860-72-5; A, 873-74-5; A ethyl carbamate derivative, 21703-06-0; H, 79121-26-9; FA, 97860-68-9; MD, 97860-69-0; PNO, 51279-53-9; Cl<sub>2</sub>CH<sub>2</sub>, 75-09-2; (TPP)Fe<sup>III</sup>Cl, 16456-81-8; HCHO, 50-00-0; ClC(O)OEt, 541-41-3; PhN(Me)CD<sub>3</sub>, 88889-00-3; *p*-CNC<sub>6</sub>H<sub>4</sub>N(CD<sub>3</sub>)<sub>2</sub>, 88889-02-5; (CH<sub>3</sub>)<sub>2</sub>C=C(CH<sub>3</sub>), 563-79-1; (*Z*)-PhCH=CHPh, 645-49-8; (*E*)-PhCH=CHPh, 103-30-0; D<sub>2</sub>, 7782-39-0; [(TPP)(Cl)Fe<sup>IV</sup>=O]<sup>+</sup>, 97877-23-1; cyclohexane, 110-82-7; cyclohexene, 110-83-8; cyclohexanol, 108-93-0; 2-cyclohexen-1-ol, 822-67-3; bicyclo[2.2.1]hept-2-ene, 498-66-8; tetramethyloxirane, 5076-20-0; 7-oxabicyclo[4.1.0]heptane, 286-20-4; 3-oxatricyclo[3.2.1.0<sup>2,4</sup>]octane, 278-74-0; *cis*-stilbene oxide, 1689-71-0; *trans*-stilbene oxide, 1439-07-2; 2,4,6-tri-*tert*-butylphenol, 732-26-3.

(47) Burka, L. T.; Guengerich, F. P.; Willard, R. J.; Macdonald, T. L. J. *Am. Chem. Soc.* 1985, 107, 2549.

## Communications to the Editor

### Trichloro(1-methylcytosinato)gold(III). Model for Gold-DNA Interactions

Marko S. Holowczak, Mark D. Stancl, and  
Geoffrey B. Wong\*

Department of Chemistry  
University of Southern California  
Los Angeles, California 90089-1062

Received January 7, 1985

Attention to gold coordination chemistry has been growing in recent years because of its relevance to the gold antiarthritic drugs and the possible antitumor properties of certain gold compounds.<sup>1-3</sup> One specific area of interest has been the interaction between DNA and gold(I) or gold(III). Studies using viscometry and UV spectroscopy suggest that AuCl<sub>4</sub><sup>-</sup> binds to DNA.<sup>4</sup> Model gold(III) complexes with various adenine derivatives have been studied chromatographically.<sup>5</sup> Complexes with guanosine and related compounds also have been isolated and characterized by NMR, infrared, and Mössbauer spectroscopies.<sup>6,7</sup> Triethylphosphino-gold(I) has recently been found to bind to DNA in a noncondensing fashion.<sup>8</sup> Complexes between gold(I) and guanosine (and the related inosine) have been partially characterized.<sup>6</sup> However, structural data have not been reported on any gold-DNA model compounds. We present here the first such complex to be characterized crystallographically, trichloro(1-methylcytosine)-gold(III).

The title compound was prepared by mixing 300 mg (0.83 mmol, 1 ml H<sub>2</sub>O) of NaAuCl<sub>4</sub> with 104 mg (0.83 mmol, 3 mL of H<sub>2</sub>O) of 1-methylcytosine (MeCyt) (Vega Biochemicals). Soon afterward, the product precipitated as a fine yellow powder. It was collected, washed with water, dried, and recrystallized from acetonitrile/isopropyl alcohol by slow evaporation: mp ~183 °C dec. Anal.<sup>9</sup> Calcd for C<sub>5</sub>H<sub>7</sub>AuCl<sub>3</sub>N<sub>3</sub>O: C, 14.02; H, 1.65. Found: 14.27; 1.68. Proton NMR (CH<sub>3</sub>CN-*d*<sub>3</sub>) δ 7.25 (br, NH<sub>2</sub>, 7.55 d, H(6)), 5.98 (d, H(5)), 3.40 (s, CH<sub>3</sub>).

Crystal data: space group *P*2<sub>1</sub>/*c*; *a* = 6.944 Å, *b* = 22.930 *c* = 13.061 Å, β = 94.54; *Z* = 8. Intensity data were collected on a Syntex P2<sub>1</sub> automated four-circle diffractometer with Mo Kα radiation. Full-matrix least-squares refinement, with anisotropic temperature factors for all non-hydrogen atoms, converged to a final *R* factor of 0.048. Two crystallographically independent molecules were located.

A view of one of the molecules is shown in Figure 1. Three chlorine atoms and the N3 define a nearly square-planar coordination geometry, which is typical for Au(III). The Au-N distance of 2.031 Å (2.039 (15) and 2.023 (16) Å) compares with other reported Au-N distances: 2.09 and 2.58 (axial) in [Au(2,9-dimethylphenanthroline)Cl<sub>3</sub>];<sup>10</sup> 2.08 and 2.61 (axial) in [Au(2,9-dimethylphenanthroline)Br<sub>3</sub>];<sup>10</sup> 1.93 (shorter for steric reasons), 2.029, and 2.018 in [Au(terpy)Cl]<sup>2+</sup>;<sup>11</sup> 1.98-2.04 in [Au(tetraphenylporphyrin)Cl];<sup>12</sup> 2.031 in [Au(1,4-benzodiazepin-2-one)Cl<sub>3</sub>];<sup>13</sup> and 2.01 in [Au(NH<sub>3</sub>)Cl<sub>3</sub>].<sup>14</sup> In Au(MeCyt)Cl<sub>3</sub> the cytosine ring lies almost perpendicular to the AuCl<sub>3</sub> plane, with a dihedral angle of 85° between the two least-squares planes. Such a large angle would be expected to minimize steric repulsion. Within the ligand, bond distances and angles appear to be relatively little affected by gold binding, although the C2-N3-C4 angle of 123° is slightly larger than the usual range for cytosines. Typically, the C2-N3-C4 and C6-N1-C2 angles are 119-121° and 119-123°, respectively, in a

\* Present address: Raychem Corporation, 300 Constitution Dr., Menlo Park, CA 94025.

- (1) Sutton, B. M. *A.C.S. Symp. Ser.* 1983, 209, 355-369.
- (2) Shaw, C. F. *Inorg. Perspect. Biol. Med.* 1979, 2, 287-355.
- (3) Simon, T. M.; Kunishima, D. H.; Vibert, G. J.; Lorber, A. *Cancer Res.* 1981, 41, 94-97.
- (4) Pillai, C. K. S.; Nandi, U. S. *Biopolymers* 1973, 12, 1431-1435.
- (5) Gibson, D. W.; Beer, M.; Barnett, R. J. *Biochemistry* 1971, 10, 3669-3679.
- (6) Hadjiladis, N.; Pneumatikakis, G.; Basosi, R. J. *Inorg. Biochem.* 1981, 14, 1155-126.
- (7) Calis, G. H. M.; Hadjiladis, N. *Inorg. Chim. Acta* 1984, 91, 203-212.
- (8) Blank, C. E.; Dabrowiak, J. C. *J. Inorg. Biochem.* 1984, 21, 21-29.

- (9) Analyses were performed by Atlantic Microlab, Atlanta, GA.
- (10) Robinson, W. T.; Sinn, E. *J. Chem. Soc., Dalton Trans* 1975, 726-731.
- (11) Hollis, L. S.; Lippard, S. J. *J. Am. Chem. Soc.* 1983, 105, 4293-4299.
- (12) Timkovich, R.; Tulinsky, A. *Inorg. Chem.* 1977, 16, 962-963.
- (13) Minghetti, G.; Foddai, C.; Cariati, F.; Ganadu, M. L.; Manassero, M. *Inorg. Chim. Acta* 1982, 64, L235-L236.
- (14) Strååle, J.; Gelinek, J.; Kölmel, M. Z. *Anorg. Allg. Chem.* 1979, 456, 241-260.